



國立臺灣大學理學院物理學系暨研究所

碩士論文

Department of Physics

College of Science

National Taiwan University

Master Thesis

單一金奈米球非線性散射之機制

Mechanism of Nonlinear Scattering of Single Gold Nanosphere

黃彥達

Huang, Yen-Ta

指導教授：朱士維 博士

Advisor: Chu, Shi-Wei, Ph.D.

中華民國 103 年 6 月

June, 2014

誌謝



在這個實驗室的兩年間，我首先要感謝的是朱士維老師。不僅是給了實驗是這個良好的環境，也在研究、做事、為人方面給我許多啟發。另外也感謝老師一直鼓勵我們參與國內外的會議及研究交換，讓我們有許多開闊視野和不同環境的學習機會。感謝張之威和林宮玄老師常常給許多研究上的建議，也感謝賀培銘老師這麼支持我突然想跳出來玩玩看的決定，並在申請學校上給予的協助。

在實驗室的同袍方面，我最感謝的是學侑，在剛進實驗室的時候耐心地回答我許多有的沒有的問題，在實驗上也很多協助及建議；感謝治原、柏輔、冠宇、恆毅、東瑜、明穎在我剛進實驗室搞不清楚狀況的時候幫助我熟悉這個環境，跟我說東西要去哪裡找；感謝哲維、運儒、冠杰、國仁、庭英、億城常常提醒和提供我必要的資訊，並陪我度過許多艱困與快樂的時光；感謝美瑜、李炫雖然常常像碎碎念的大嬸，卻讓我有許多閒話家事的樂趣；感謝毓婷、冠郁、柏宣、柏廷優秀地協助交接，問了許多有趣我卻漏掉的問題；感謝瑋冠、天祥、致雍、文翊讓實驗室添增許多年輕的熱鬧。

大阪大学に研究交換の期間、一番感謝するのは藤田克昌先生です。藤田先生は私に知識とアドバイスを教えてくれるし、大事な研究の熱情もみせてくれました。研究について、庄司先生、山中さん、増井さん、亮達さん、成柏翰、米丸さん、望月さん、Imad、桶谷さん、関谷さんの色々な手伝ったにととても感謝しました。清滝さん、浦野さん、牛場さん、畔堂さん、渡辺さん、國久さん、奥野さん、田口さん、上垣さん、小林さん、藤原さん、加茂さんの生活サポートと文化交流（居酒屋などXD）、ほんどうにありがとうございました！

最後，我還要感謝我女朋友跟家人。如果沒有他們生活和情感上的協助，我大概沒有辦法這麼悠哉地唸書和研究。



中文摘要



不久之前，單一金奈米粒子的飽和及可壓制散射特性剛剛才被發現[1]。飽和散射指的是散射率到某一個光強度時會開始減弱；而可壓製散射則是我們可以用一道光來壓制另一道不同波長光的散射率。這兩個現象都是以連續波雷射觀察到的。藉著這兩種非線性現象，無光致褪色的超解析顯微術已經被實現[2]。儘管我們觀察到這樣的現象與局域表面電漿子共振有很強的波長相關性，其物理機制卻尚未被完全了解。在本論文中，我們回顧過去在飽和及可壓制散射的實驗結果，接著引入 $\chi^{(3)}$ 模型以描述這個單一金奈米粒子非線性散射的特性。我們做了一系列不同波長(405~700nm)、大小(直徑 20~80nm)及偏振的散射實驗與此模型擬合。這些實驗結果顯示我們觀察到的光學非線性由局域表面電漿子共振所增強，且其大小與其非線性程度有很大的正相關性。我們沒有觀察到可見的偏振相關性。在考慮有可能的微觀非線性來源後，單一金奈米粒子由連續波雷射觀察到的飽和及可壓制散射唯一可能的來源是熱光效應，也就是金的晶格溫度造成的。

關鍵字：金奈米粒子、光、非線性、散射

ABSTRACT



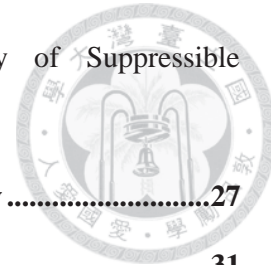
Previously, saturable and suppressible scattering[3] of single gold nanosphere have been reported. Saturable scattering means the decreasing reflectance as intensity of incident laser reached certain threshold; suppressible scattering means that one laser beam can suppress the reflectance of another laser with different wavelength. Both phenomena are based on continuous wave laser. Based on these nonlinearities ,non-bleaching superresolution microscopies are realized [2]. Although it has been shown that saturation intensities depend on the wavelengths and localized surface plasmon resonance band, the mechanism of the nonlinear scattering is still unclear. In this thesis, we first summarize our previous experimental results of saturable and suppressible scattering. In small particle limit $\chi^{(3)}$ model is introduced to fit with experimental results of nonlinear scattering by single gold nanosphere. We have performed extensive wavelength (405~700nm), sizes (diameter 20~80nm), and polarization studies to characterize nonlinear scattering in a single nanoparticle. The results show the optical nonlinearity is enhanced by localized surface plasmon resonance, and the size is positively related to the nonlinearity behavior. No polarization dependence was observed. After extensive discussion of the possible candidates for microscopic mechanism, saturable and suppressible of gold nanosphere by continuous wave laser are attributed to thermo-optical effect, i.e. hot lattice of gold.

CONTENTS



口試委員會審定書	#
誌謝	i
中文摘要	iii
ABSTRACT	iv
CONTENTS	v
LIST OF FIGURES	vii
Chapter 1 Introduction.....	1
1.1 Why Gold Nanoparticle?.....	1
1.1.1 Localized Surface Plasmon Resonance	1
1.1.2 Chemical Stability	8
1.2 Saturable and Reverse Saturable Scattering.....	12
1.3 Suppressible and Reverse Suppressible Scattering.....	14
1.4 Goal and Outline	16
Chapter 2 $\chi^{(3)}$ Model of Nonlinear Scattering Sphere in Small Particle Limit ..	17
2.1 Saturable Scattering	17
2.2 Suppressible Scattering	20
2.3 Quantitative Parameters to Characterize Nonlinear Scattering	22
Chapter 3 Wavelength and Size Dependency of Saturable Scattering	24
3.1 Wavelength Dependency	24
3.2 Size Dependency	25

Chapter 4	Wavelength, Size, and Polarization Dependency of Suppressible Scattering	27
4.1	Suppression Spectrum & Polarization Dependency	27
4.2	Size Dependency of Suppression Spectrum	31
Chapter 5	Microscopic Mechanisms	34
5.1	Candidates	Error! Bookmark not defined.
5.1	Instantaneous Nonlinear Polarizations	34
5.2	Hot Electron	35
5.3	Hot Lattice	37
Chapter 6	Conclusion	42
REFERENCE		43



LIST OF FIGURES



- Fig. 1-1 Sketch of a nanosphere shined by laser beam with wavelength much larger than the radius. a is the radius, \vec{E} is the electric field, ϵ is the dielectric constant of gold, and ϵ_M is the dielectric constant of the matrix material. In this limit, the nanosphere feels uniform electric field at every instant.2
- Fig. 1-2 Dielectric constant for gold in optical region, summarized in [9]. Because the real part of relative dielectric constant is negative, the $|S_0|^2$ will resonant with incident wave when the real part of the denominator approaches zero.7
- Fig. 1-3 Q_{sca} of 20 nm and 80 nm GNSs. The black curve shows the exact Mie solution, and the red curve is the approximate solution in small particle limit ($x = ka = 2\pi \frac{a}{\lambda} \ll 1$).....7
- Fig. 1-4 The process of the creation and decay of surface plasmon polariton, with the scattering process omitted. [12-17].....9
- Fig. 1-5 Reflectance vs Intensity curve of 80 nm GNS, using CW 561 nm laser. Reflectance is defined as backward scattering divided by incident intensity, normalized by 1 in linear extreme. Here we call the decreasing region as saturable scattering (SatS), and the increasing region as reverse-saturable scattering (RSatS). The linear fitting $1 - S_s$ will be explained in section 2.3.14
- Fig. 1-6 Example of suppressible and reverse suppressible scattering. The increasing intensity of 592 nm suppresses and reversely suppresses the scattering of 543 nm.15

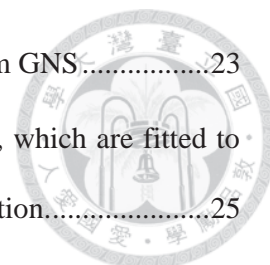


Fig. 2-1 The approximate field enhancement factor $|f|$ of 80nm GNS.....23

Fig. 3-1 Saturation Slope versus Wavelength for GNSs of 80nm, which are fitted to the cubic of the field enhancement $|f|$, after normalization.....25

Fig. 3-2 Saturation Slope versus Size for several different wavelengths, which shows that larger GNSs have stronger optical nonlinearity.....26

Fig. 4-1 Setup for measuring suppression spectrum of GNSs28

Fig. 4-2 Linear scattering spectrum of single 80nm GNS, experimental result compared with Mie solution. The experimental result is the average of 5 different GNS.....29

Fig. 4-3 Suppression spectrum by CW 561nm of 80nm GNS, averaged over 4 GNSs.30

Fig. 4-4 1– Reflectance plotted with the cubic of field enhancement $|f|$31

Fig. 4-5 Suppression spectrum of 60nm GNS by CW 561nm laser.....32

Fig. 4-6 Suppression spectrum (1– Reflectance) fitted with the field enhancement of 80nm and 60nm GNSs.....33

Fig. 5-1 Reflectance v.s. peak intensity for 80nm GNS by 520nm, 500fs pulse laser.35

Fig. 5-2 Wavelength dependency of saturable scattering of 80nm GNSs fitted with $\chi_r^{(3)}$ model from hot lattice.....38

Fig. 5-3 Reflectance of single gold nanosphere at different temperatures, normalized by the scattering spectrum at 30°C.....41

Chapter 1 Introduction



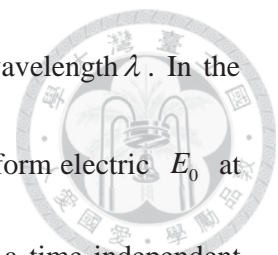
1.1 Why Gold Nanoparticle?

Gold nanoparticles (GNP) are widely used since ancient time for the beautiful colors[4]. Now we understand that the colors are dominated by localized surface plasmon resonance, and the resonance attracts even more interests in recent decades, mainly for its potentials in various applications from its strong field enhancement in optical region[5]. Gold is one of the most favorable materials for its excellent chemical stability. In this section, we briefly summarize the advantages of GNP as a nonlinear material, and depict the calculation of localized surface plasmon resonance in small particle limit for the nonlinear model in later chapter.

1.1.1 Localized Surface Plasmon Resonance

Localized surface plasmon resonance (LSPR) is a kind of resonant phenomena between light and nanoparticle, which will enhance the field strength around and increase the cross section of scattering/absorption. Thus, the optical nonlinearity will also be enhanced. In the case of noble metal nanoparticles, the resonant wavelengths are from ultraviolet to infrared. In theory, people need to resort to different approximations and simulation methods to predict quantitatively in complicated geometry. Fortunately, analytic solutions by Maxwell equations are possible in some highly symmetric geometry. The sphere case was solved beautifully by Mie, and Bohren & Huffman's book [6] is a good review. In order to construct the model of scattering of single gold nanosphere with nonlinear polarization later, the case of sphere in small particle limit is presented briefly here.

Consider a sphere of dielectric constant ϵ with radius a immersed in dielectric



material ϵ_m , shined with incident plane electromagnetic wave of wavelength λ . In the small particle limit $\frac{\lambda}{a} \ll 1$, and the sphere approximately feels uniform electric E_0 at any specific time. Thus, the Maxwell equation may be written to a time-independent form (where \vec{D} is electric displacement, \vec{E} is electric field, \vec{H} is magnetic field strength, and \vec{B} is magnetic field):

$$\begin{aligned}
 \nabla \cdot \vec{D} &= 0 \\
 \nabla \cdot \vec{B} &= 0 \\
 \nabla \times \vec{E} &= \frac{\partial \vec{B}}{\partial t} = 0 \\
 \nabla \times \vec{H} &= \frac{\partial \vec{D}}{\partial t} = 0
 \end{aligned}
 \tag{1.1}$$

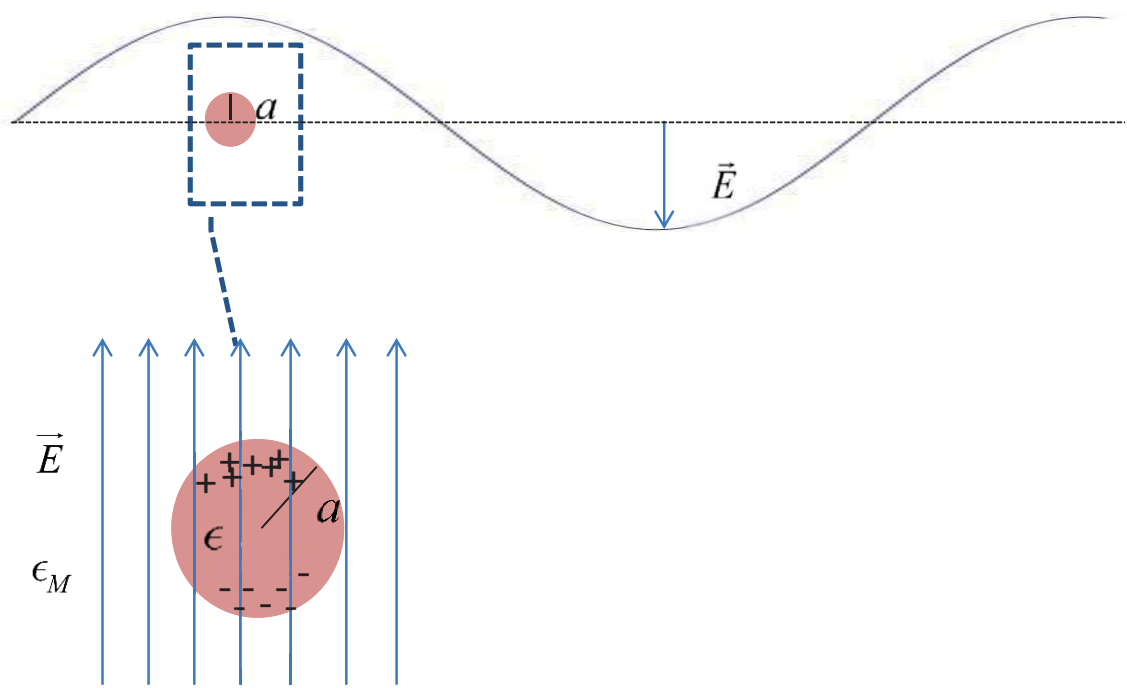
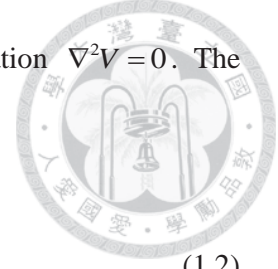


Fig. 1-1 Sketch of a nanosphere shined by laser beam with wavelength much larger than the radius. a is the radius, \vec{E} is the electric field, ϵ is the dielectric constant of gold, and ϵ_M is the dielectric constant of the matrix material. In this limit, the nanosphere feels uniform electric field at every instant.

dielectric material $\vec{D} = \epsilon \vec{E}$, it returns to the usual Poisson equation $\nabla^2 V = 0$. The rotational symmetry gives us:



$$\begin{aligned} V_{out} &= \sum_{l=0}^{\infty} \left[a_l r^l + \frac{b_l}{r^{l+1}} \right] P_l(\cos \theta) \\ V_{in} &= \sum_{l=0}^{\infty} c_l r^l P_l(\cos \theta) \end{aligned} \quad (1.2)$$

where the $1/r^{l+1}$ terms are absent in V_{in} to avoid divergence around $r=0$. Because the boundary condition $V_{out} \rightarrow -E_0 r \cos \theta = -E_0 r^{l=1} P_{l=1}(\cos \theta)$ for $r \rightarrow \infty$ contains only the $l=1$ mode, we would expect the solution only containing $l=1$ terms:

$$\begin{aligned} V_{out} &= \left[-E_0 r + \frac{b}{r^2} \right] \cos \theta \\ V_{in} &= cr \cos \theta \end{aligned} \quad (1.3)$$

After fitting the boundary condition at $r=a$ with $V_{in} = V_{out}$ and $\vec{D}_{in} \cdot \hat{r} = \vec{D}_{out} \cdot \hat{r}$, we get:

$$\begin{aligned} V_{out} &= -\left[1 - \frac{\epsilon_r - 1}{\epsilon_r + 2} \frac{a^3}{r^3} \right] E_0 r \cos \theta = -\left[1 - f_1 \frac{a^3}{r^3} \right] E_0 r \cos \theta \\ V_{in} &= -\frac{3}{\epsilon_r + 2} E_0 r \cos \theta = -f_2 E_0 r \cos \theta \end{aligned} \quad (1.4)$$

where V_{out} and V_{in} correspond to the V out of and in the sphere, $\epsilon_r = \epsilon / \epsilon_M$ is the dielectric constant relative to the surrounding material, $f_1 := \frac{\epsilon_r - 1}{\epsilon_r + 2}$, $f_2 := \frac{3}{\epsilon_r + 2}$, and

E_0 is the uniform electric field far from sphere as a boundary condition. By calculating the surface bound charge[7]:

$$\begin{aligned} \sigma_b &= \epsilon_0 (\mathbf{E}_{in} - \mathbf{E}_{out}) \cdot \hat{r} \\ &= -3\epsilon_0 f_1 E_0 \cos \theta \\ &= S \cos \theta \end{aligned} \quad (1.5)$$

where $S = -3\epsilon_0 f_1 E_0$. Then we are able to calculate the dipole moment:



$$\begin{aligned}
 p_z &= \hat{z} \int \sigma_b z dA \\
 &= \hat{z} \int S \cos \theta (a \cos \theta) (a^2 d(\cos \theta) d\phi) \\
 &= \frac{4\pi a^3}{3} S \hat{z} \\
 &= VS \hat{z}
 \end{aligned} \tag{1.6}$$

,where V is the volume of sphere, and assuming the incident wave with polarization in z direction. For electromagnetic wave, we have $E_0 = |E_0| e^{-i\omega t}$. By the formula of differential cross section of dipole radiation[7],

$$\begin{aligned}
 \frac{d\sigma_{scat}}{d\Omega} &= \sum_{\hat{e}} \frac{k^4}{(4\pi\epsilon_0 |E_0|)^2} |\hat{e}^* \cdot \vec{p}|^2 \\
 &= \frac{k^4 V^2}{(4\pi\epsilon_0 |E_0|)^2} |S|^2 (0 + \sin^2 \theta) \\
 &= k^4 a^6 |f_1|^2 \sin^2 \theta
 \end{aligned} \tag{1.7}$$

where the \hat{n} is the unit of vector in the direction of detection, and \hat{e} is the polarization of detection. Here we summed over two directions of polarization (although one of them is 0). We may also integrate it into total cross section,

$$\begin{aligned}
 \sigma_{scat} &= k^4 a^6 |f_1|^2 2\pi \int_{-1}^1 \sin^2 \theta d(\cos \theta) \\
 &= 2\pi k^4 a^6 |f_1|^2 \left[2 - \frac{2}{3}\right] \\
 &= \frac{8}{3} x^4 A |f_1|^2
 \end{aligned} \tag{1.8}$$

where we define $x = ka$ and $A = \pi a^2$ as the physical cross section of the sphere. Sometimes it is convenient to define dimensionless cross section by normalizing it with the physical cross section[6],

$$Q_{sca} = \frac{\sigma_{sca}}{A} = \frac{8}{3} x^4 |f_1|^2 = \frac{8}{3} x^4 \left| \frac{\epsilon_r - 1}{\epsilon_r + 2} \right|^2 \tag{1.9}$$

In the case of normal dielectric material with small dispersion, the $|f_1|^2$ part changes only slightly with wavelength, but the $x^4 \propto 1/\lambda^4$ gives us Rayleigh scattering. In the

case of metal, however, the real part of dielectric constant can be negative in some frequency, so the denominator of $|f_1|^2$ can be close to zero. This leads to the “resonance” between the electromagnetic wave and the nanoparticle around specific frequency, which is usually called localized surface plasmon resonance (LSPR). Because the field is composed of strong coupling between electromagnetic wave and free electron, the corresponding quantization is often called surface plasmon polariton. For example, the Fig. 1-2 shows the dielectric constant of gold relative to vacuum (or simply $\epsilon_{gold} / \epsilon_0$). For a small gold nanosphere (GNS) immersed in immersion oil ($\epsilon_{oil} = n^2 \epsilon_0 \approx (1.518)^2 \epsilon_0 \approx 2.304 \epsilon_0$), the real part of $(\epsilon_r + 2)$ will be approximately zero for wavelength around $540nm$. The red curve in Fig. 1-3 shows the result of calculation, where the peak LSPR is apparent.

If we want to consider larger particles, higher order corrections need to be taken into account. The exact Mie solution is given in [6], and we only cite the result here:

$$\begin{aligned}
 Q_{sca} &= \frac{2}{x^2} \sum_{n=1}^{\infty} (2n+1) (|a_n|^2 + |b_n|^2) \xrightarrow{x \ll 1} \frac{8}{3} x^4 \left| \frac{m^2 - 1}{m^2 + 2} \right|^2 = \frac{8}{3} x^4 |f_1|^2 \\
 Q_{ext} &= \frac{2}{x^2} \sum_{n=1}^{\infty} (2n+1) \text{Re}(a_n + b_n) \\
 Q_{abs} &= Q_{ext} - Q_{sca} \xrightarrow{x \ll 1} 4x \text{Im} \left[\frac{m^2 - 1}{m^2 + 2} \right] = 4x \text{Im}[f_1]
 \end{aligned} \tag{1.10}$$

where Q_{sca} , Q_{ext} , and Q_{abs} are the normalized cross sections of scattering, extinction, and absorption, and the other parameters are given by



$$\begin{aligned}
a_n &:= \frac{m\psi_n(mx)\psi'_n(x) - \psi_n(x)\psi'_n(mx)}{m\psi_n(mx)\xi'_n(x) - \xi_n(x)\psi'_n(mx)} \\
b_n &:= \frac{\psi_n(mx)\psi'_n(x) - m\psi_n(x)\psi'_n(mx)}{\psi_n(mx)\xi'_n(x) - m\xi_n(x)\psi'_n(mx)} \\
x &:= ka \\
m &:= \sqrt{\epsilon_r} \\
\psi_n(\rho) &:= \rho j_n(\rho) \\
\xi_n(\rho) &:= \rho h_n^{(1)}(\rho)
\end{aligned} \tag{1.11}$$

where $j_n(\rho)$ are the spherical Bessel functions of 1st kind, and $h_n^{(1)}(\rho)$ are the spherical Hankel functions of 1st kind. We will leave the discussion of absorption later and concentrate on scattering here. The scattering cross sections of exact solutions are plotted as black curve in Fig. 1-3, taking 20nm and 80nm GNSs for example. It is seen that the small particle limit is a good approximation for 20nm, but deviates from exact solution noticeably in the case of 80nm. To confirm the validity of exact Mie solution, we measured the scattering spectrum of single 80nm gold nanosphere by the setup depicted in section 4.1. The result is as Fig. 4-2, which fitted very well with Mie solution.

In fact, we should notice the “resonance” much earlier when we see the factors f_1 and f_2 in (1.4), both of which will enhance for the same reason. The electric field inside $\vec{E}_{in} = f_2 \vec{E}_0$ will get an enhancement factor of f_2 right away. This field enhancement is so useful that some new fields of applications are open, e.g. surface-enhanced Raman scattering [8]. For us, the field enhancement is important because it will enhance the effect of nonlinearity, and thus affect the scattering by laser beam of high intensity.

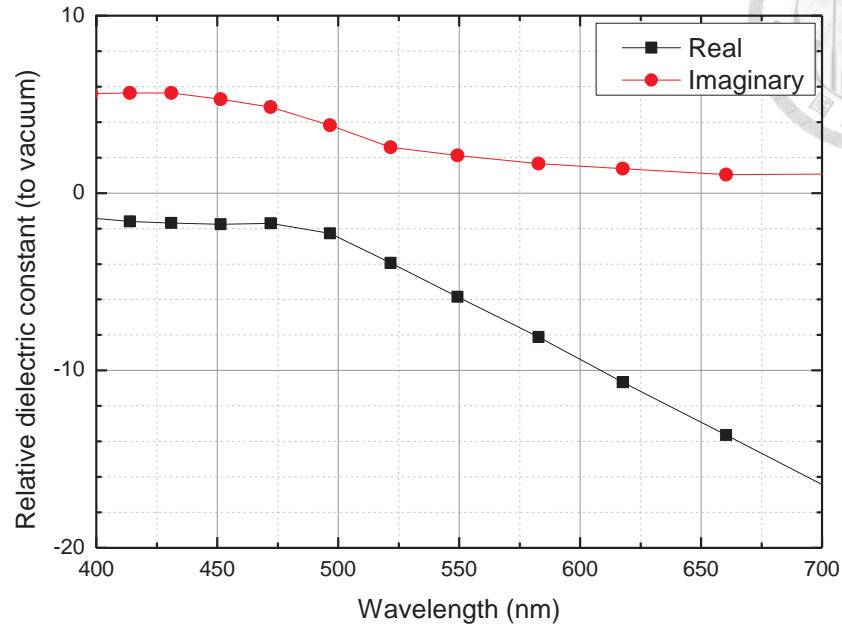
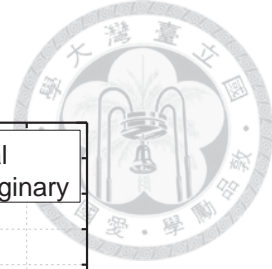


Fig. 1-2 Dielectric constant for gold in optical region, summarized in [9]. Because the real part of relative dielectric constant is negative, the $|S_0|^2$ will resonate with incident wave when the real part of the denominator approaches zero.

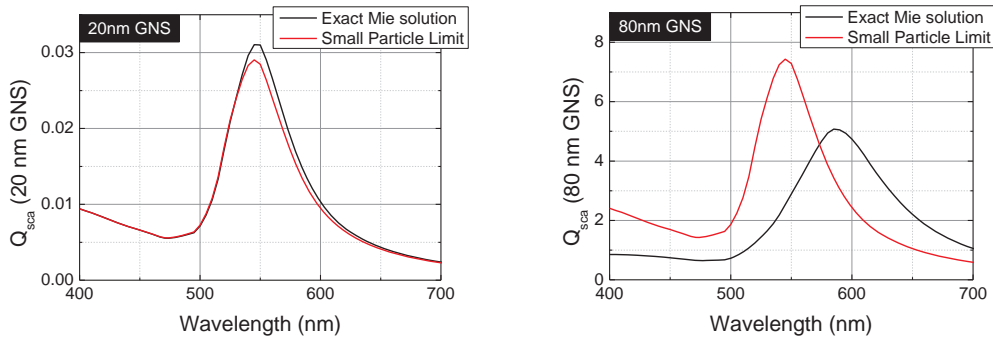
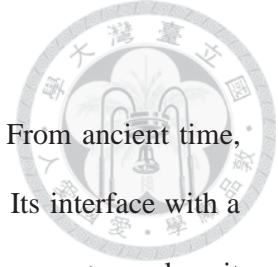


Fig. 1-3 Q_{sca} of 20 nm and 80 nm GNSs. The black curve shows the exact Mie solution, and the red curve is the approximate solution in small particle limit

$$(x = ka = 2\pi \frac{a}{\lambda} \ll 1)$$



1.1.2 Chemical Stability

Gold has long been known to be one of the most stable materials. From ancient time, people used gold for currency, accessory, and the sign of nobleness. Its interface with a fluid and a gas is the least reactive among metals[10]. This property makes it competitive in many potential application, such as those in vitro[11]. In this thesis, we also consider the gold nanoparticle in usual dielectric materials, such as glass and immersion oil. Thus we do not expect to see any chemical reaction.

1.2 Temporal Information of Localized Surface Plasmon

In the literature, the behaviors of surface plasmon polariton in metallic nanoparticle have been researched by pump-probe experiments thoroughly[12-14]. One of the best review was given by Link's paper[14]. In brief, the surface plasmon polariton is excited and the correlated electron motion is in quasi-equilibrium with laser beam in the first few femtoseconds[13]; in the time scale of sub-picosecond, the surface plasmon polariton decays due to electron-electron coupling and electron-phonon coupling ($\tau_{e^-e^-} \sim 0.5ps$, $\tau_{e^-ph} \sim 1ps$ for gold[15]), which thermalize the energy distribution of electrons and heat up the lattice; finally, the heat is relaxed to the matrix on a hundred pico-second depending on the surrounding material[13,16,17] (refer to Fig. 1-4).

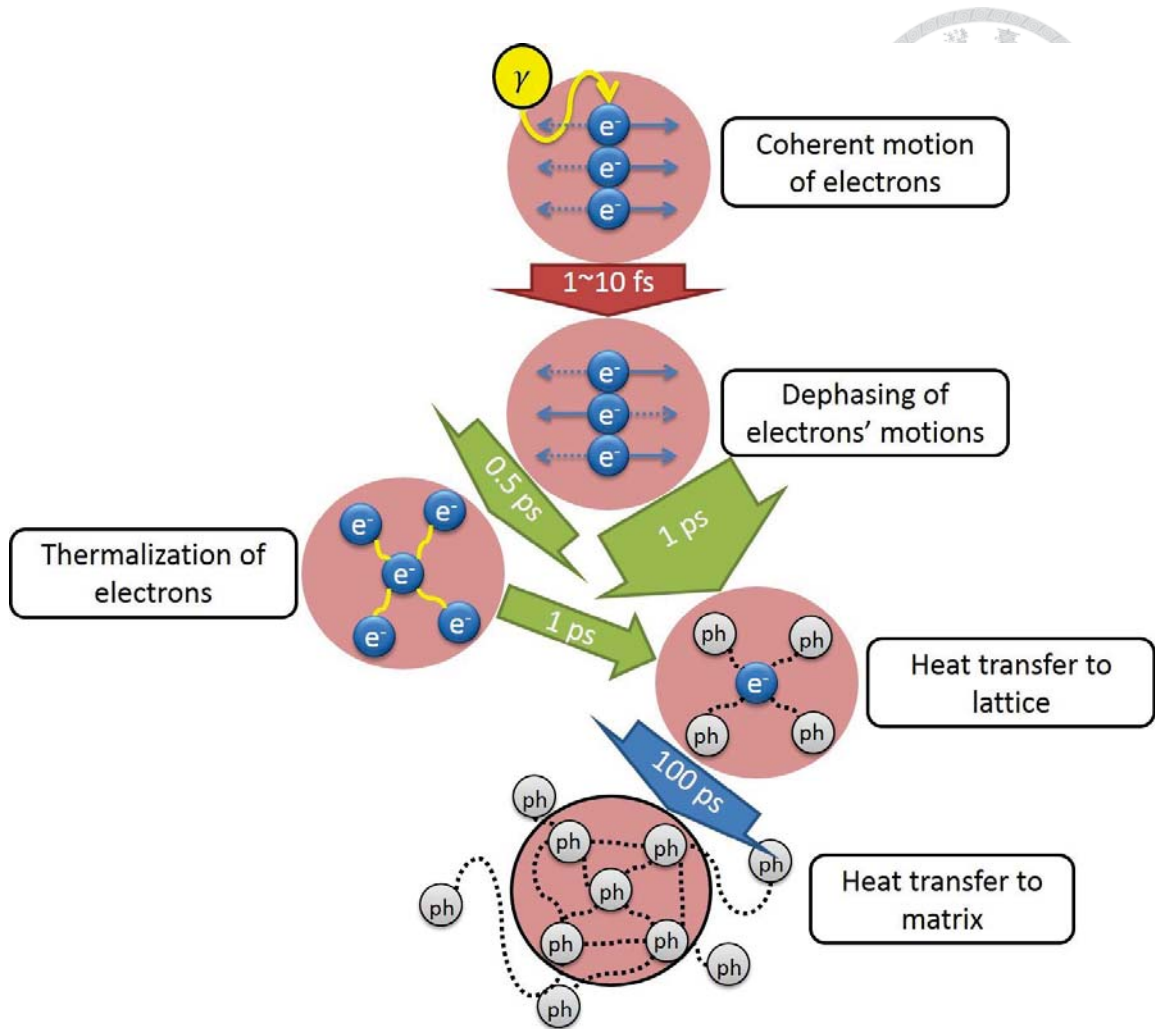
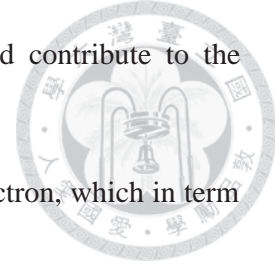


Fig. 1-4 The process of the creation and decay of surface plasmon polariton, with the scattering process omitted. [12-17]

1.3 Optical Nonlinearity of Gold Nanoparticle

From the process of the decay of localized surface plasmon in previous section, there are several mechanisms that may cause optical nonlinearity of gold nanoparticle: (in this thesis, I will focus our discussion of optical nonlinearity on the process without harmonic generation, such as second harmonic generation. No other wavelength is produced within the sensitivity of our spectrometer in our experiments.)

1. In exciting surface plasmon polariton, the third order nonlinear polarization from



interband[18] or intraband transition[19] (Kerr nonlinearity) could contribute to the scattering.

2. The rising temperature of electron or lattice could change the electron, which in turn change the dielectric constant[18].

3. The energy relaxed to lattice causes the temperature rise of gold lattice, and thus changes the corresponding dielectric constant.

One of the easiest way to measure the optical nonlinearity is through measuring the nonlinear absorption by Z-scan-method[20,21]. In brief, a laser is focused to have z-directional dependency of intensity, and the sample is scanned through different z to measure the intensity dependency of the absorption of laser beam. It was found that when the intensity reaches the order of $10^9 W / cm^2$, the absorption will decrease a little first, and then increase sharply afterward. These phenomena are usually called saturable absorption and reverse-saturable absorption respectively, from the imagination that the plasmon band is saturated and cannot be absorbed anymore just like fluorescence (although there is no rigorous way corresponds to the analogy[22]). This method is both easy to use and cheap, but the lack of temporal information makes it hard to distinguish the nonlinearities from different mechanisms. In addition, many particles are measured at the same time, where the non-uniform samples might cause problem.

There are several cleaner ways to observe all of the mechanisms above separately by different experiments in the literature before. In the following, a brief review of the corresponding experiments will be given.

1.3.1 Third Order Nonlinear Polarization

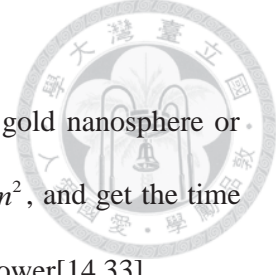
According to quantum mechanics, higher order nonlinear polarization of electron will be induced in strong electric field[23]. The third order nonlinear polarization is the lowest order effect producing the same frequency. In the case of gold, the third order

nonlinearity includes both intraband and interband transition in optical frequency, which may be calculated by relativistic augmented-plane-wave method[24]. Because the nonlinear polarization is almost instantaneous compared with single laser pulse (usually >10 fs), the temporal width is usually the same as the pulse width of laser[14].

One of the cleanest ways to measure the signal from third order is by the degenerate four-wave-mixing[18,25-27]. Briefly speaking, the same pulse laser beam is divided into three beams, and the beams are focused on the sample with different wave vectors $\vec{k}_{1,2,3}$. A new nonlinear polarization of the same frequency $\omega = \omega - \omega + \omega$ will be induced in the direction of $\vec{k}_4 = \vec{k}_1 + \vec{k}_2 - \vec{k}_3$ will be induced, so a new beam of different direction will be observed without mixed up with the previous three laser beam[23]. Delay lines may also be used to extract the temporal information of signal. Because the signal comes from the coherent collective motions of electron, the lifetime is only of the order of several fs as dephasing time T_2 [23,25,28,29].

1.3.2 Hot Electron

On the electron-electron scattering on the time scale of 0.5 ps[30], electron thermalization occurs and the high temperature of electrons could change the dielectric constant[18]. In pump-probe experiment, the temperature of electrons depends on the fluence of single pulse and the timescale of electron-phonon scattering. In the case of gold film, pump-probe measurement of reflectivity can be applied to see the electron-temperature's effect on dielectric constant[15,30]. The temporal information of electron-electron scattering is assumably the same for both bulk of gold and gold nanoparticle[14]. Many people also makes use of the pump-probe of absorption (or equivalently transmittance) to get the temporal information of absorption[31] or its spectrum[22]. Most of the experiments measured the response of ensemble of gold



nanoparticle, instead of single particle.

Totally speaking, the experiments observing hot electron effect of gold nanosphere or colloid made use of the laser about $fluence / area \approx 0.01 \sim 0.1 J / cm^2$, and get the time scale of $\tau_{e-e} = 0.5 \sim 1 ps$ [14,15,20,32,33] depending on the laser power[14,33].

It should be noted that the timescale of electron-phonon scattering, $\tau_{e-ph} \approx 1 \sim 5 ps$, is about the same as electron-electron scattering. These two relaxation paths are usually competing effects and are fitted using double exponential function[14,15]. This makes the two nonlinearities overlap and hard to be separated. In this thesis, we will call the combination as hot electron.

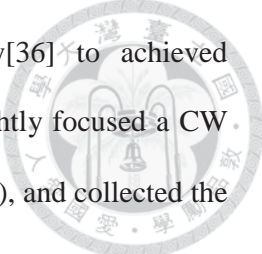
1.3.3 Hot Lattice

When the energy absorbed is further relaxed to lattice through electron-phonon scattering, the temperature of lattice rises and the dielectric constant changes. Typically the changes of dielectric constant will decrease the absorption. The time-scale of the change of dielectric constant is decided by phonon-phonon relaxation, i.e. energy relaxed from gold nanoparticles to the matrix, and is typically of the order of 100ps[14], measured by pump-probe experiment of absorption. The decrease of absorption is dominated by LSPR for different wavelengths, and the ratio of decrease may be up to the order of 10% at $72^\circ C$ [34], for 22nm gold nanoparticle.

Note that this effect could strongly depends on size because the temperature rise is positively related to the size of particles under the same laser intensity[35]. This is also confirmed by our experiment in later chapter.

1.4 Saturable and Reverse Saturable Scattering

Previous, we observe the nonlinear scattering of single gold nanoparticle embedded in dielectric material by continuous wave laser for the first time to our knowledge[3], and



also successful applied it with saturated excitation microscopy[36] to achieved non-photo bleaching superresolution microscopy[2]. In brief, we tightly focused a CW laser beam on a single gold nanoparticle immersed in oil ($n_m \approx 1.518$), and collected the backward scattering light. We chose the wavelength near the LSPR peak to obtain the maximum field enhancement. In linear case, the ratio of the scattered light to incident intensity, which we call reflectance here, should be constant (normalized to 1). However, when the intensity increases to about 10^6 W/cm^2 , the reflectance will decrease to lower than 50%, and then bouncing back to more than 130% if the excitation intensity further increases (see Fig. 1-5). A very similar trend can be found in figure 3(b) in Elim's paper[31], which reported saturable & reverse saturable absorption (SatA & RSatA) and of ensemble gold nanoparticles. The similar trends of absorption and scattering might imply the same physical mechanism between these measurements. Following the convention in absorption, we called our observation saturable & reverse saturable scattering (SatS & RSatS) to describe the decreasing of reflectance in the case of high intensity.

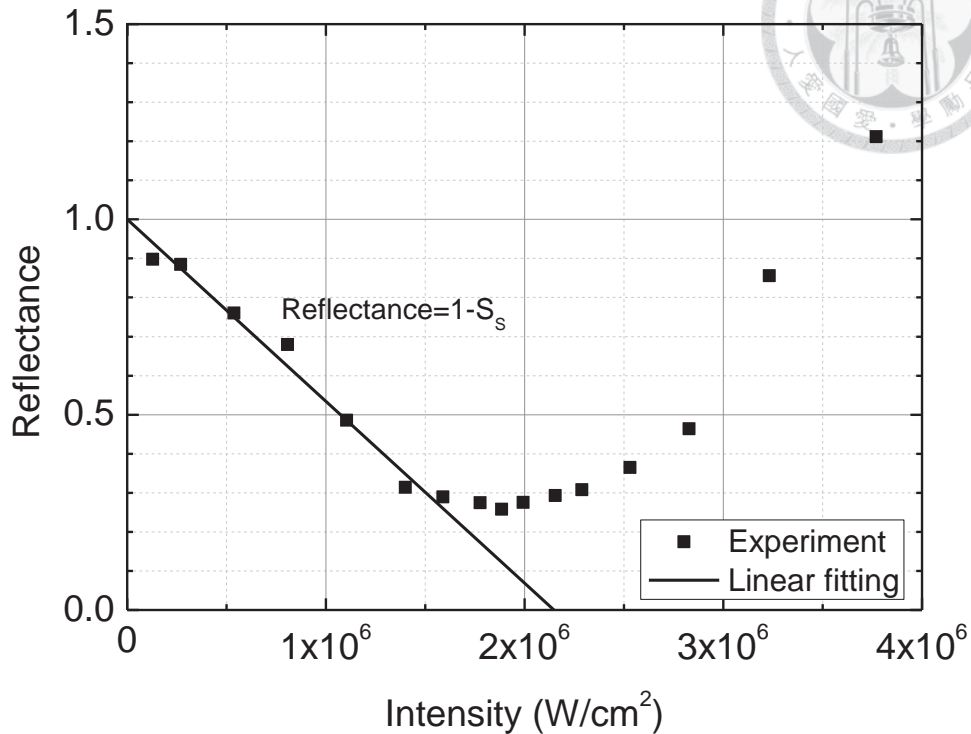
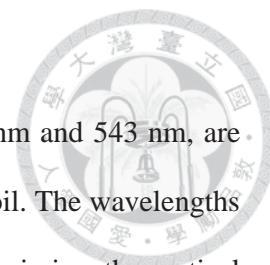


Fig. 1-5 Reflectance vs Intensity curve of 80 nm GNS, using CW 561 nm laser. Reflectance is defined as backward scattering divided by incident intensity, normalized by 1 in linear extreme. Here we call the decreasing region as saturable scattering (SatS), and the increasing region as reverse-saturable scattering (RSatS). The linear fitting $1-S_s$ will be explained in section 2.3.

1.5 Suppressible and Reverse Suppressible Scattering

After getting saturable and reverse saturable scattering, it is interesting that whether the same nonlinearity can be used to control one light by another. The potential applications include optical switching and superresolution. In Wu, Hsueh-Yu's master thesis, the suppressible & reverse suppressible scattering (SupS & RSupS) of one laser beam by another is shown, and the superresolution using the method of saturated emission depletion microscopy was demonstrated. Here I only briefly depict the nonlinear



behavior.

In the setup, two circular polarized laser beam of wavelength 592 nm and 543 nm, are aligned and focused on single 80 nm GNS immersed in immersion oil. The wavelengths were chosen to be close to the LSPR band (Fig. 1-3), to maximize the optical nonlinearity. In this example, we used strong 592 nm laser beam as the pump to induce nonlinearity and weak 543 nm as the probe. The result is shown in Fig. 1-6. With increasing intensity of 592 nm, the reflectance of 543 nm is suppressed to lower than 20%, and then reversely suppressed at higher intensity. This tendency is very similar to the SatS and RSatS, as can be seen from the curves. The intensity of this phenomenon is also consistent with the saturable and reverse saturable scattering of the 592 nm itself, which strongly implies the same mechanism.

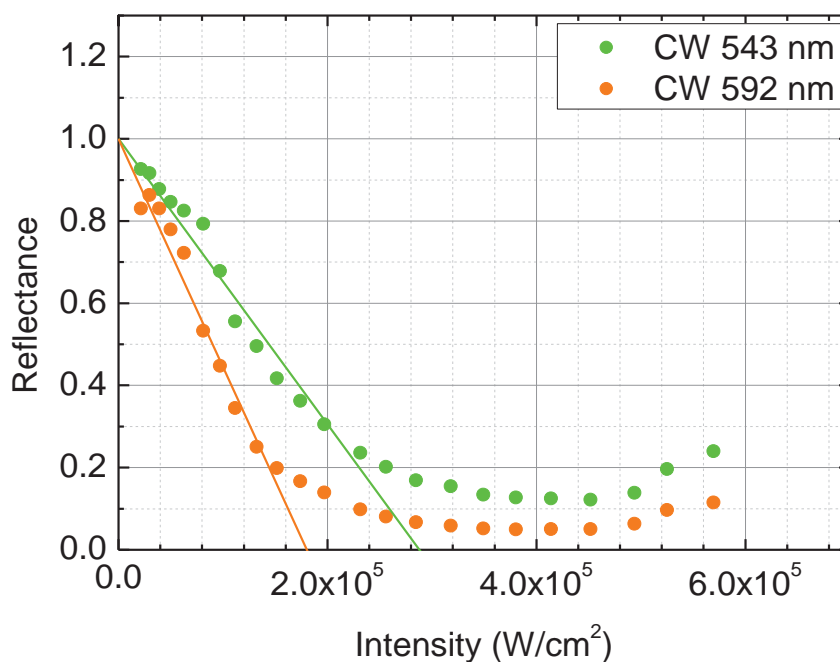
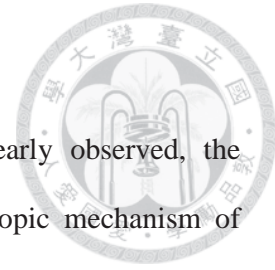


Fig. 1-6 Example of suppressible and reverse suppressible scattering. The increasing intensity of 592 nm suppresses and reversely suppresses the scattering of 543 nm.

1.6 Goal and Outline

Although the phenomena of nonlinear scattering have been clearly observed, the underlying mechanism is still unclear. To determine the microscopic mechanism of saturable and suppressible scattering, it will be helpful to have systematic information of wavelength, size, and polarization dependency of saturable and suppressible scattering. In addition, a model of nonlinear scattering is wanted for fitting.

In Chapter 2, the model of nonlinear scattering of single GNS in small particle limit is given. The experimental results of saturable and suppressible scattering under Chapter 3 and Chapter 4, including different sizes of GNSs and changing wavelength & polarization of laser beam. We will discuss about various microscopic mechanisms available in the literature, and rule out some of them for the nonlinear scattering observed in Chapter 5.



Chapter 2 $\chi^{(3)}$ Model of Saturable and Suppressible Scattering Sphere in Small Particle Limit



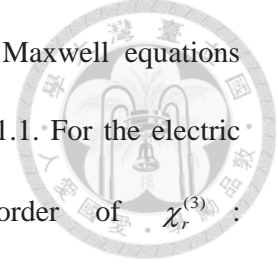
In order to quantitatively compare the saturable scattering of GNS for different wavelengths and sizes, we need a model with nonlinear parameter to fit with. In previous chapter, we see that Mie solution, deduced by Maxwell equations, is consistent with our experimental spectrum. Thus, it is reasonable using Maxwell equations with nonlinear dielectric constant $\chi^{(3)}$ to phenomenologically describe the nonlinear scattering in classical level. However, it is difficult to calculate the exact solution for large particle to all orders of $\chi^{(3)}$, partly because Mie solution has already use perturbation for large particle. To simplify the question, we calculate the scattering of GNS with nonlinear dielectric constant $\chi^{(3)}$ in small particle limit. Both the models of saturable scattering and suppressible scattering are shown.

2.1 Saturable Scattering

Consider a GNS of radius a with relative dielectric constant $\epsilon_r = \epsilon / \epsilon_M$ in dielectric material ϵ_m . In the limit of $\lambda \gg a$, we have the same Maxwell equations as (1.1), except that we want to have nonlinear electric displacement in the GNS:

$$\begin{aligned} \overline{D}_{in} &= \epsilon_M [\epsilon_r + \chi_r^{(3)}(\omega = \omega - \omega + \omega) | \overline{E}_{in} |^2] \overline{E}_{in} \\ \overline{D}_{out} &= \epsilon_M \overline{E}_{out} \end{aligned} \quad (2.1)$$

Note that the $\chi_r^{(3)}(\omega = \omega - \omega + \omega)$ here can be either instantaneous or



non-instantaneous in the present. For electric field outside, the Maxwell equations returns to Poisson equation $\nabla^2 V_{out} = 0$ with $\overline{E}_{in} = -\nabla V_{in}$, as in 1.1.1. For the electric field inside, we expand the electric field in the order of $\chi_r^{(3)}$: $\overline{E}_{in} = \overline{E}_{in}^{(0)} + \overline{E}_{in}^{(1)} + \overline{E}_{in}^{(2)} + \overline{E}_{in}^{(3)} + \dots$, and plug it into $\nabla \cdot \overline{D}_{in} = 0$. Because ∇ is zero order of $\chi_r^{(3)}$ and $\nabla \times \overline{E}_{in} = 0$, we can also write $\overline{E}_{in}^{(n)} = -\nabla V_{in}^{(n)}$. Grouping the terms by the order of $\chi_r^{(3)}$ (and to make it concise, neglect the vector notation), we get:

$$\begin{aligned}
0 &= (1/\epsilon_M)\nabla \cdot D_{in} \\
&= \left\{ \epsilon_r \nabla \cdot E_{in}^{(0)} \right\} \\
&+ \left\{ \epsilon_r \nabla \cdot E_{in}^{(1)} + \chi_r^{(3)} \left[\nabla \cdot (|E_{in}^{(0)}|^2 E_{in}^{(0)}) \right] \right\} \\
&+ \left\{ \epsilon_r \nabla \cdot E_{in}^{(2)} + \chi_r^{(3)} \left[\nabla \cdot (|E_{in}^{(0)or(1)}|^2 E_{in}^{(0)or(1)}) \right] \right\} \\
&+ \left\{ \epsilon_r \nabla \cdot E_{in}^{(3)} + \chi_r^{(3)} \left[\nabla \cdot (|E_{in}^{(0)or(1)or(2)}|^2 E_{in}^{(0)or(1)or(2)}) \right] \right\} \\
&+ \dots
\end{aligned} \tag{2.2}$$

where the $E^{(0)or(1)or(2)}$ terms mean all the combination possible with $E^{(0)}$, $E^{(1)}$, or $E^{(2)}$ plugging into the same place. Because this equation is perturbatively true, every order (curly bracket) must be zero separately. For the 0th order, the equation returns to the Poisson equation in previous chapter. According to (1.4), $E_{in}^{(0)} = f_2 E_0 \hat{z}$. Plug the $E_{in}^{(0)}$ into the 1st order bracket, we get $\nabla \cdot E_{in}^{(1)} = -\nabla^2 V_{in}^{(1)} = 0$, which is Poisson equation for $V_{in}^{(1)}$ again. For the same reason as (1.3), we will get:

$$\begin{aligned}
V_{out}^{(0)} + V_{out}^{(1)} &= - \left[1 - [f_1 + C] \frac{a^3}{r^3} \right] E_0 r \cos \theta \\
V_{in}^{(0)} + V_{in}^{(1)} &= - [f_2 + D] E_0 r \cos \theta
\end{aligned} \tag{2.3}$$

where we already separate some factors out for convenience. This gives us constant electric field $E_{in}^{(1)} = D E_0 \hat{z}$, and when plug it into the 2nd order terms, the equation gives us $\nabla \cdot E_{in}^{(2)} = -\nabla^2 V_{in}^{(2)} = 0$ again. We can do this procedure iteratively, and the result

gives us (after fitting the boundary conditions):

$$\begin{aligned} V_{out} &= -\left[1 - [f_1 + C] \frac{a^3}{r^3}\right] E_0 r \cos \theta \\ V_{in} &= -[f_2 - C] E_0 r \cos \theta \end{aligned} \quad (2.4)$$



where $C = \frac{Xf_2}{3}(f_2 - C) |f_2 - C|^2$ and $X = \chi_r^{(3)} E_0^2$. By calculating the boundary

charge:

$$\begin{aligned} \sigma_b &= \epsilon_0 (\mathbf{E}_{in} - \mathbf{E}_{out}) \cdot \hat{r} \\ &= \epsilon_0 [f_2 - C - 1 - 2(f_1 + C)] E_0 \cos \theta \\ &= -3\epsilon_0 [f_1 + C] E_0 \cos \theta \\ &= S \cos \theta \end{aligned} \quad (2.5)$$

we may calculate the scattering cross section as before:

$$\begin{aligned} Q_{sca} &= \frac{8}{3} x^4 |f_1 + C|^2 \\ &= \frac{8}{3} x^4 |f_1|^2 \left|1 + \frac{C}{f_1}\right|^2 \end{aligned} \quad (2.6)$$

This is our exact scattering cross section with nonlinear $\chi_r^{(3)}$. If we want to the perturbative nonlinear behavior, $C \sim 0$ and can be given by:

$$\begin{aligned} C &= \frac{Xf_2}{3}(f_2 - C) |f_2 - C|^2 \\ &\sim \frac{Xf_2}{3}(f_2 - 0) |f_2 - 0|^2 \\ &\sim \frac{f_2^2 |f_2|^2}{3} X \end{aligned} \quad (2.7)$$

To compare with the experimental results, we may define reflectance as the scattering cross section normalized by linear region:



$$\begin{aligned}
\text{Reflectance} &:= \frac{Q_{sca}}{Q_{sca,linear}} = \left| 1 + \frac{C}{f_1} \right|^2 \\
&\xrightarrow{x \ll 0} \left| 1 + \frac{f_2^2 |f_2|^2}{3f_1} X \right|^2 \\
&\sim 1 + \text{Re} \left[\frac{2f_2^2 |f_2|^2}{3f_1} \chi_r^{(3)} |E_0|^2 \right]
\end{aligned} \tag{2.8}$$

Note that $f_1 := \frac{\epsilon_r - 1}{\epsilon_r + 2}$ and $f_2 := \frac{3}{\epsilon_r + 2}$ are the resonant factor of LSPR, which means

that the nonlinear behavior of saturable scattering should also be resonant, with third order of f_1 and f_2 . To test the validity of this $\chi_r^{(3)}$ model, we will need to know wavelength dependency of saturable scattering.

2.2 Suppressible Scattering

In order to describe suppressible scattering, we need the interaction term between two different frequencies. Define ω_{probe} (ω_{pump}) and E_{probe} (E_{pump}) as the angular frequency and electric field of probe (pump) respectively. Field enhancement factors

$$f_{pump,1} := \frac{\epsilon_{r,pump} - 1}{\epsilon_{r,pump} + 2} \quad (f_{probe,1} := \frac{\epsilon_{r,probe} - 1}{\epsilon_{r,probe} + 2}) \quad \text{and} \quad f_{pump,2} := \frac{3}{\epsilon_{r,pump} + 2} \quad (f_{probe,2} := \frac{3}{\epsilon_{r,probe} + 2})$$

are defined as f_1 and f_2 in previous section, for pump (probe) wavelength. If the pump is weak, we may write the electric displacement of ω perturbatively as:

$$\begin{aligned}
D_{probe,in} &= \epsilon_m \left[\epsilon_{r,probe} + \chi_r^{(3)} (\omega_{probe} = \omega_{probe} + \omega_{pump} - \omega_{pump}) |E_{pump,in}|^2 \right] E_{probe,in} \\
&= \epsilon_m \left[\epsilon_{probe,r} + \delta\epsilon_{probe,r} \right] E_{probe,in} \\
D_{probe,out} &= \epsilon_m E_{probe,out}
\end{aligned} \tag{2.9}$$

Which is exactly the same situation as the linear case, except that the $\epsilon_{probe,r}$ is replaced by $\epsilon_{probe,r} + \delta\epsilon_{probe,r}$. The pump-dependency of $\delta\epsilon_{probe,r}$ is through $E_{pump,in}$,

given by (2.4) as $E_{pump,in} = [f_{pump,2} - C] E_{pump,0} \hat{z}$ and



$C = \frac{Xf_{pump,2}}{3} (f_{pump,2} - C) |f_{pump,2} - C|^2$. According to (1.9), the scattering cross section is

given by:

$$\begin{aligned} Q_{sca} &= \frac{8}{3} x^4 \left| \frac{\epsilon_{probe,r} + \delta\epsilon_{probe,r} - 1}{\epsilon_{probe,r} + \delta\epsilon_{probe,r} + 2} \right|^2 \\ &= \frac{8}{3} x^4 \left| f_{probe,1} + \frac{1}{3} f_{probe,2}^2 \delta\epsilon_{probe,r} + O(\delta\epsilon_{probe,r}^2) \right|^2 \end{aligned} \quad (2.10)$$

We may also define the reflectance as in (2.8):

$$\begin{aligned} \text{Reflectance} &:= \frac{Q_{sca}}{Q_{sca,linear}} = \left| \frac{\epsilon_{probe,r} + \delta\epsilon_{probe,r} - 1}{\epsilon_{probe,r} + \delta\epsilon_{probe,r} + 2} \right|^2 / \left| \frac{\epsilon_{probe,r} - 1}{\epsilon_{probe,r} + 2} \right|^2 \\ &= \left| 1 + \frac{1}{3} \frac{f_{probe,2}^2}{f_{probe,1}} \delta\epsilon_{probe,r} + O(\delta\epsilon_{probe,r}^2) \right|^2 \\ &= 1 + \text{Re} \left[\frac{2f_{probe,2}^2}{3f_{probe,1}} \chi_r^{(3)} |E_{pump,in}|^2 \right] + O(\delta\epsilon_{probe,r}^2) \\ &= 1 + \text{Re} \left[\frac{2f_{probe,2}^2}{3f_{probe,1}} \chi_r^{(3)} |f_{pump,2}|^2 |E_{pump,0}|^2 \right] + O(\delta\epsilon_{probe,r}^2) \end{aligned} \quad (2.11)$$

This form is very similar to (2.8), except that the saturation is a self-suppression process.

Through the factor $|f_{pump,2}|^2$, we can see that if the pump wavelength is close to LSPR

resonant, the suppression would be stronger; in addition, the suppression will also be

stronger for the probe wavelength close the LSPR peak, from the factor of $\frac{f_{probe,2}^2}{f_{probe,1}}$.

The suppression here has an intuitive explanation in large-field limit: for

$|E_{pump,0}|^2 \rightarrow \infty$,

$$\begin{aligned} \text{Reflectance} &= \left| \frac{\epsilon_{probe,r} + \delta\epsilon_{probe,r} - 1}{\epsilon_{probe,r} + \delta\epsilon_{probe,r} + 2} \right|^2 / \left| \frac{\epsilon_{probe,r} - 1}{\epsilon_{probe,r} + 2} \right|^2 \\ &\rightarrow 1 / \left| \frac{\epsilon_{probe,r} - 1}{\epsilon_{probe,r} + 2} \right|^2 = 1 / |f_{probe,1}|^2 \end{aligned} \quad (2.12)$$

The resonant term approaches 1 due to the large dielectric constant, and thus the



Reflectance becomes the inverse of field enhancement factor $1/|f_{probe,1}|^2$.

2.3 Quantitative Parameters to Characterize Nonlinear Scattering

In previous sections, we depict the nonlinear scattering of single gold nanosphere with $\chi_r^{(3)}$, for single laser beam or suppression between two. In order to confirm the validity of this model, it is natural to ask whether the wavelength dependency is consistent with experimental results or not.

Observing Fig. 1-5, the degree of nonlinearity reflects in the deviation from constant reflectance 1. Perturbatively speaking, we may fit the deviation from 1 with a linear function, and define the slope as saturation slope (or suppression) slope S_{sat} (S_{sup}):

$$\text{Reflectance} = 1 - S_{sat \text{ or } sup} I \quad (2.13)$$

With the relation between intensity and the square of electric field $I = \epsilon_M |E_0|^2 v / 2 = \epsilon_0 c n_M |E_0|^2 / 2$, where v is the velocity of light in the matrix's material, we may get the saturation and suppression slope from (2.8) and (2.11):

$$\begin{aligned} S_{sat} &= -\text{Re}\left[\frac{4f_2^2 |f_2|^2}{3c\epsilon_0 n_M f_1} \chi_r^{(3)}(\omega = \omega - \omega + \omega)\right] \\ S_{sup} &= -\text{Re}\left[\frac{4f_{probe,2}^2 |f_{pump,2}|^2}{3c\epsilon_0 n_M f_{probe,1}} \chi_r^{(3)}(\omega_{probe} = \omega_{probe} - \omega_{pump} + \omega_{pump})\right] \end{aligned} \quad (2.14)$$

This gives us the wavelength dependency of saturation and suppression slope, which is strengthened by LSPR as described in previous sections. However, the f_1 and f_2 are the field enhancement factors which are well-defined only in small particle limit. For larger particle, the electric field is in general non-uniform, which makes the calculation difficult. In order to have an approximation, we assume that $|f| := |f_1| \approx |f_2|$ and

$Q_{sca} = \frac{8}{3}x^4 |f|^2$ (which was given in small particle limit in (1.9)) even for larger particle. In this sense, we are able to calculate $|f|$ reversely from the exact Mie solution (1.10). As an example, Fig. 2-1 shows the $|f|$ of 80nm GNS, approximated by the method just described. In addition, we neglect the phase information and replace f , $\chi_r^{(3)}$ with $|f|$, $|\chi_r^{(3)}|$ as an approximation for order of magnitude. Based on this assumption, the equation (2.14) becomes:

$$\begin{aligned}
 |S_{sat}| &\approx \frac{4}{3c\epsilon_0 n_M} |f|^3 |\chi_r^{(3)}(\omega = \omega - \omega + \omega)| \\
 |S_{sup}| &\approx \frac{4}{3c\epsilon_0 n_M} |f_{pump}|^2 |f_{probe}| |\chi_r^{(3)}(\omega_{probe} = \omega_{probe} - \omega_{pump} + \omega_{pump})|
 \end{aligned} \tag{2.15}$$

By measuring the wavelength dependency of saturable and suppressible scattering, we may be able to test the validity of this model, as presented in Chapter 3 and Chapter 4.

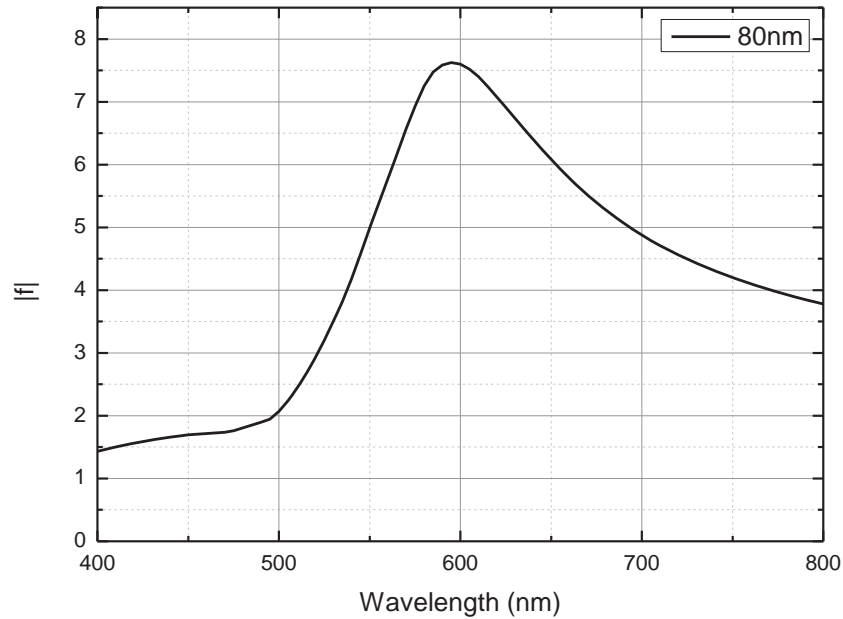


Fig. 2-1 The approximate field enhancement factor $|f|$ of 80nm GNS

Chapter 3 Wavelength and Size Dependency of Saturable Scattering



In order to confirm the validity of the $\chi^{(3)}$ model in previous chapter and understand the physical mechanism of the saturable scattering, we did the experiment by several different wavelengths of lasers, including 405nm (iBEAM-SMART-405-S-HP, Topica Photonics, Germany), 561nm (Cobolt Jive™ 561nm, Cobolt, Sweden), 592nm (Fiber Laser 592, Leica TCS SP5 system, Leica, Germany), 700nm (3900S CW Tunable Ti:Sapphire Laser, Spectra-Physics, United States), and sizes of GNSs (20, 40, 60, 80 nm diameters, Gold Colloid, BBInternational, United Kingdom).

3.1 Wavelength Dependency

Fig. 3-1 shows the results of SS versus wavelength for 80 nm's GNSs. It is apparent that the peaks of saturation slope lie at the same wavelength as the peak of field enhancement spectrum, around 550 nm to 600 nm. Here we still have no pre-knowledge about the dispersive behavior of $\chi^{(3)}$, so assume it to be constant to fit with experimental data. Based on this assumption, it fits reasonably well with the theoretical calculation of saturable scattering by $\chi^{(3)}$ model (equation (2.15)),

$$|S_{sat}| \approx \frac{4}{3c\epsilon_0 n_M} |f|^3 |\chi_r^{(3)}(\omega = \omega - \omega + \omega)|$$

The resonance here is dominated by the field enhancement factor $|f|^3$. Thus, the closer the wavelength is to the LSPR peak, the stronger the nonlinearity is. We may also inversely calculate the corresponding $|\chi^{(3)}|$ from the fitting, which gives us

$$|\chi_r^{(3)}| \approx \frac{4c\epsilon_0 n_M}{3} \frac{|S_{sat}|}{|f|^3} \sim 5.4 \times 10^{-14} \text{ (SI unit) for 80 nm GNS and } |\chi_r^{(3)}| \sim 8.2 \times 10^{-15} \text{ (SI$$

unit) for 40 nm GNS.

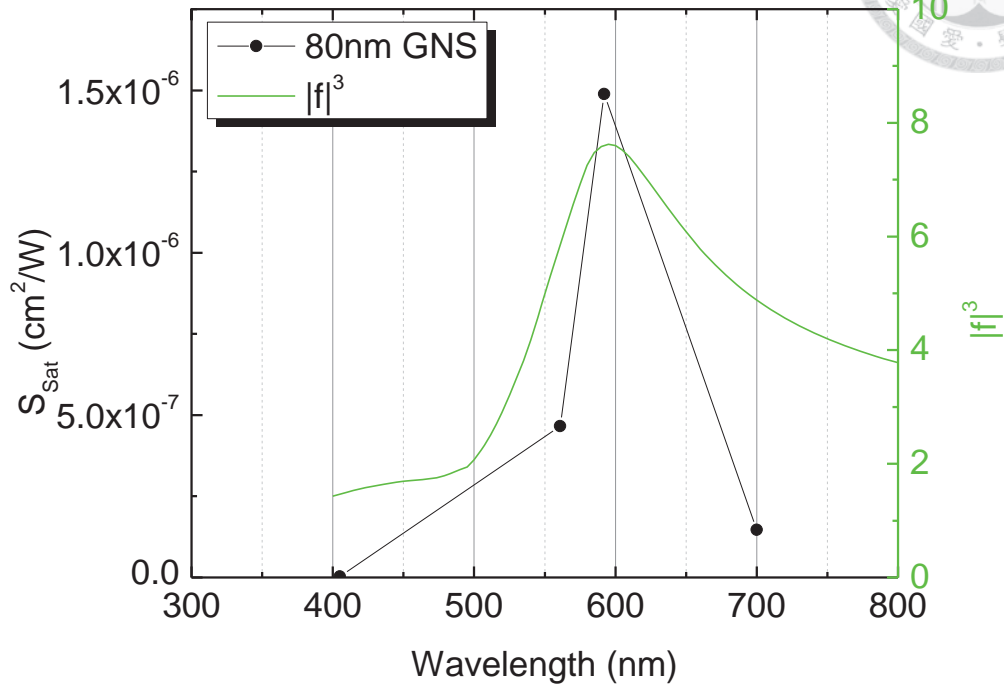
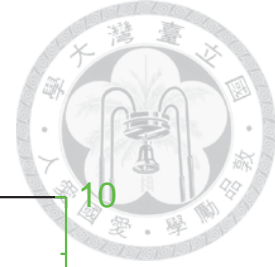


Fig. 3-1 Saturation Slope versus Wavelength for GNSs of 80nm, which are fitted to the cubic of the field enhancement $|f|$, after normalization.

3.2 Size Dependency

Although the $\chi^{(3)}$ model explains the wavelength dependency of saturable scattering, the microscopic mechanism of $\chi^{(3)}$ is not clear for us. In order to get more hints, we measure the nonlinear scattering of several sizes of GNSs. The results are shown in Fig. 3-2. An apparent tendency is that the nonlinearity grows with the sizes of GNSs.

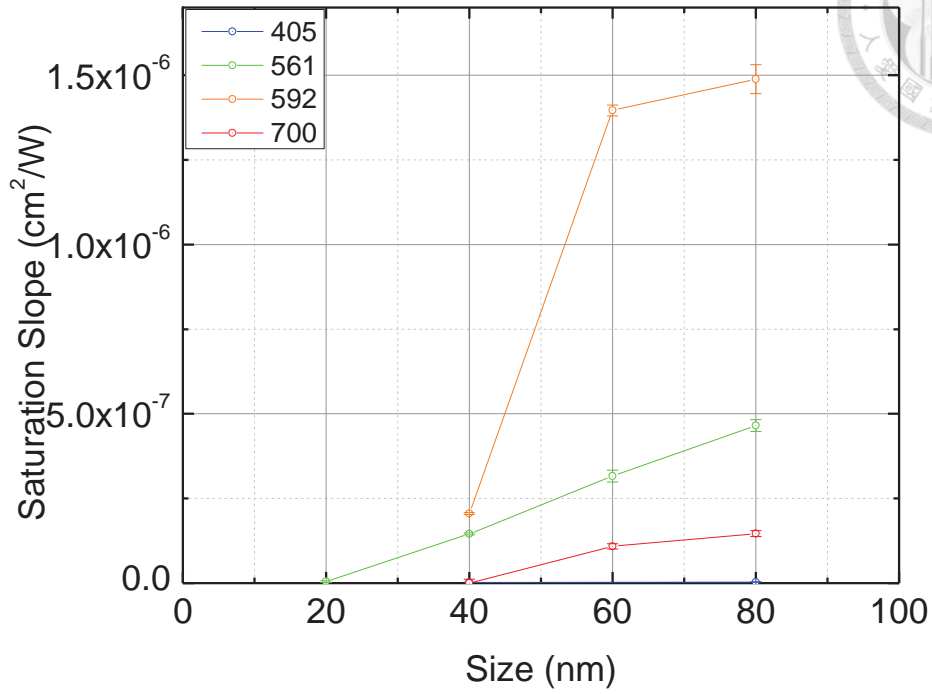
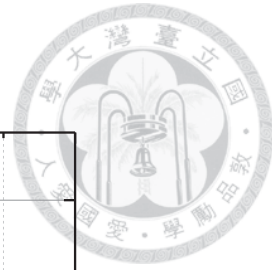


Fig. 3-2 Saturation Slope versus Size for several different wavelengths, which shows that larger GNSs have stronger optical nonlinearity

Chapter 4 Wavelength, Size, and Polarization

Dependency of Suppressible Scattering



In previous chapter, the wavelength dependency of saturable scattering gave us positive evidence of the validity of the $\chi^{(3)}$ model in section 2.1. However, we can only have few discrete data points due to the limit of high power continuous wave (CW) lasers. In this sense, suppression is more suitable for measuring wavelength dependency, because there are fewer requirements to be the suppressed laser beam. In fact, we may even use super-continuum (SC) source for continuous wavelength dependent suppression. Here we call it suppression spectrum. To extract more information, we also tune the polarizations of 561nm and SC so that they are mutually parallel or perpendicular. We will show the experimental data of our results in this line.

4.1 Suppression Spectrum & Polarization Dependency

In order to know the wavelength dependency and polarization dependency of suppressible scattering, we tried to suppress SC laser (SC400-2-PP, Fianium, United Kingdom) by CW 561nm laser (Cobolt Jive™ 561nm, Cobolt, Sweden). The setup is as Fig. 4-1.

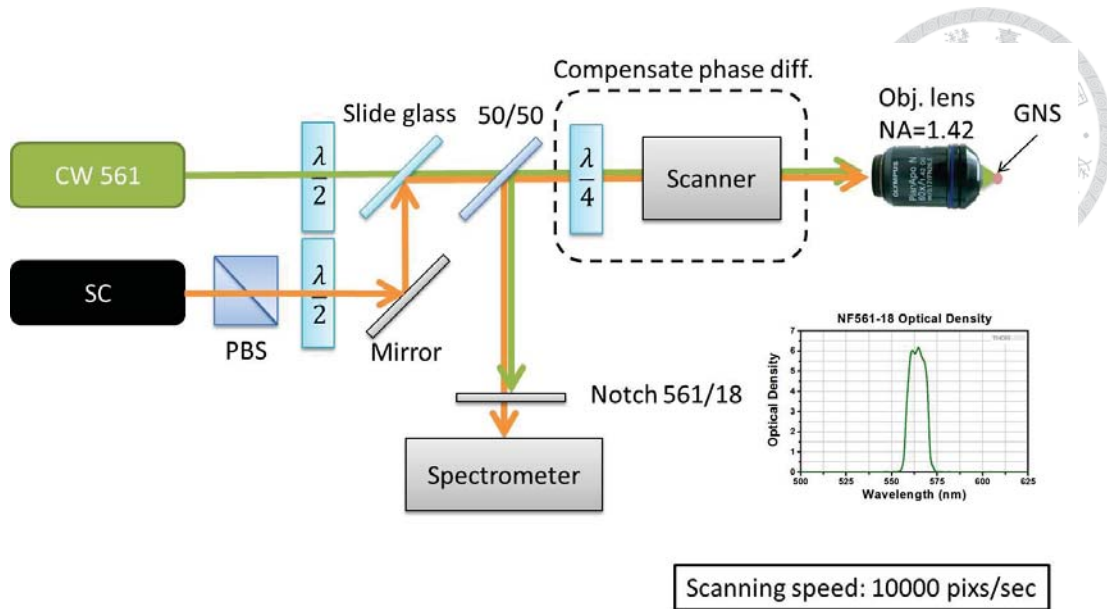


Fig. 4-1 Setup for measuring suppression spectrum of GNSs

In the setup, polarization beam splitter is used right after the SC to make it linear polarized. After passing through half-wave plate, which is used to tune the wanted polarization, CW 561nm and SC are combined together by a slide glass. The beam pass through a 50/50 beam splitter (BSW10, Thorlabs, United States), go through a broadband quarter wave plate (AQWP05M-600, Thorlabs, United States) and a homemade silver mirror based 4f scanner system, and be focused by an apochromatic objective lens (UPlanSApo 100XO, NA 1.40, Olympus, Japan) on single GNS (80nm Gold colloid, BBInternational, United States). The quarter wave plate is tuned that it will compensate the phase difference between two polarizations, caused by the silver mirror in scanner system. In the detection part, we measured the backward scattering collected by the same objective and reflected by the 50/50 beam splitter. After a notch filter of 561nm (NF561-18, Thorlabs, United States) blocking the strong 561nm scattering away, we detect the scattering spectrum by a spectrometer (Shamrock 163 & iDus DV420A-OE, Andor Technology, United Kingdom). In order to confirm the reliability of the system and the GNS sample we first measure the linear scattering

spectrum without 561nm (and notch filter), as in Fig. 4-2. The result fit well with the Mie solution, calculated by (1.10).

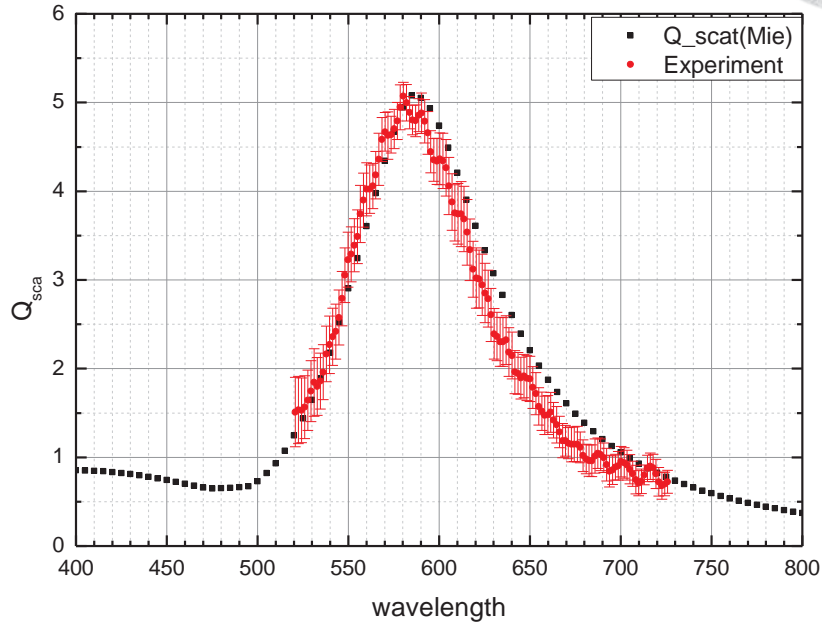
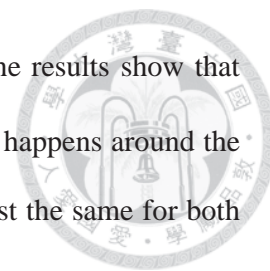


Fig. 4-2 Linear scattering spectrum of single 80nm GNS, experimental result compared with Mie solution. The experimental result is the average of 5 different GNS. After the confirmation of system, the 561 nm laser is turned on and increased the intensity gradually. The power intensity of SC is kept as low as possible to prevent the nonlinear or heating effect caused by it. After every measurement, the 561 is turned off and the linear scattering spectrum is measured again in order to prevent the damage of GNSs. The scattering spectrum with 561nm laser is normalized by the scattering spectrum without it, which is defined as reflectance by the same logic as (2.11). In the scattering is linear, the scatter spectrum should be constantly 1, independent of the intensity of 561nm. However, when the intensity increased to higher than 10^5 W/cm^2 , the spectrum will be suppressed. Fig. 4-3 shows the result for



$Intensity \approx 6.6 \times 10^5 W / cm^2$, averaged over four different GNSs. The results show that the maximum suppression of reflectance is up to about 20%, which happens around the peak of LSPR (refer Fig. 2-1). In addition, suppression rate is almost the same for both parallel and perpendicular polarizations.

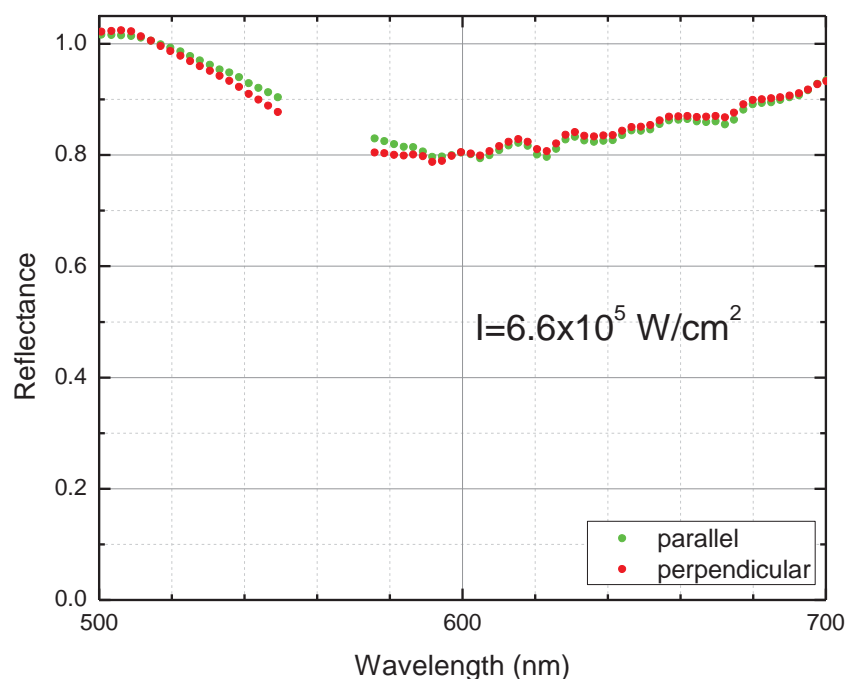
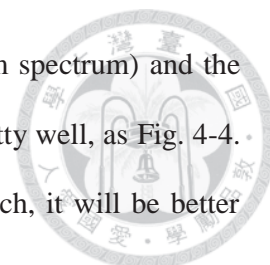


Fig. 4-3 Suppression spectrum by CW 561nm of 80nm GNS, averaged over 4 GNSs.

According to previous result of suppressing CW 543nm by CW 592 in Fig. 1-6, where both wavelengths are within LSPR peak, the decrease of reflectance was about the same. According to the saturation curve of CW 561 in Fig. 1-5, the reflectance at the intensity of $6.6 \times 10^5 W / cm^2$ is about 80%, which is compatible with the data presented here. The wavelength dependency of suppression is also consistent with the result of $\chi^{(3)}$ model in section 2.3: suppression slope should be maximized around the peak of field



enhancement. In fact, if the 1-Reflectance (calculated by spectrum spectrum) and the field enhancement (by (2.14)) are plotted together, the peaks fit pretty well, as Fig. 4-4. In application, if we want a good suppression rate for optical switch, it will be better that both wavelengths are close to LSPR peak.

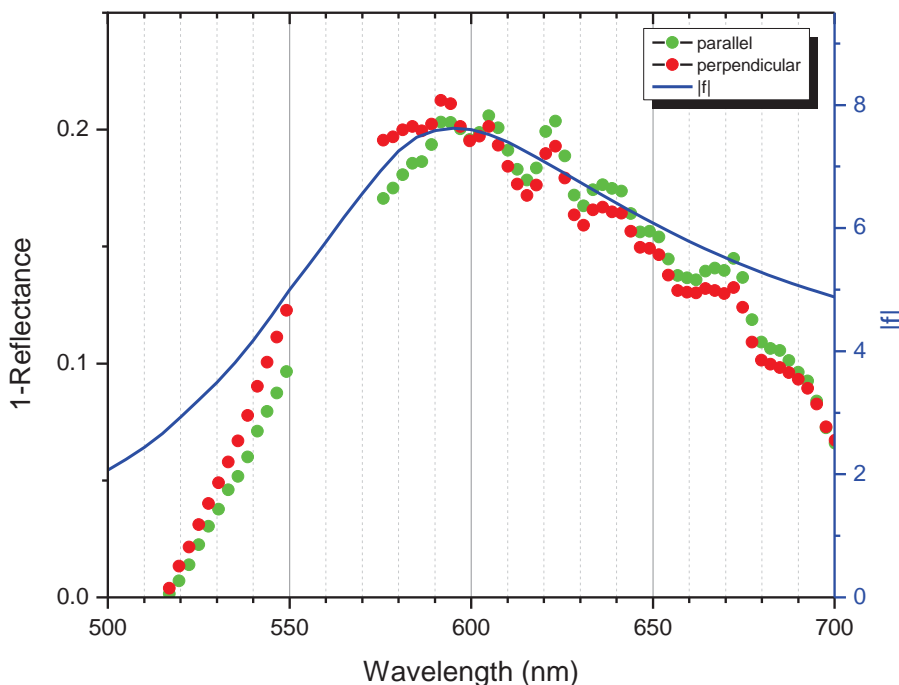


Fig. 4-4 1-Reflectance plotted with the cubic of field enhancement $|f|$.

It is very interesting to know that the suppression seems to be independent of polarization: for instantaneous nonlinear polarization, $\chi_{xxx}^{(3)}$ is in general different from $\chi_{xyy}^{(3)}$ [18,37]. This implies that our $\chi^{(3)}$ is non-instantaneous. More detail will be discussed in Chapter 5.

4.2 Size Dependency of Suppression Spectrum

To double check that the suppression spectrum is directly related to the LSPR field enhancement spectrum, we measure also measured it with 60nm GNSs. The results,

averaged with 4 GNSs, is shown in Fig. 4-5.

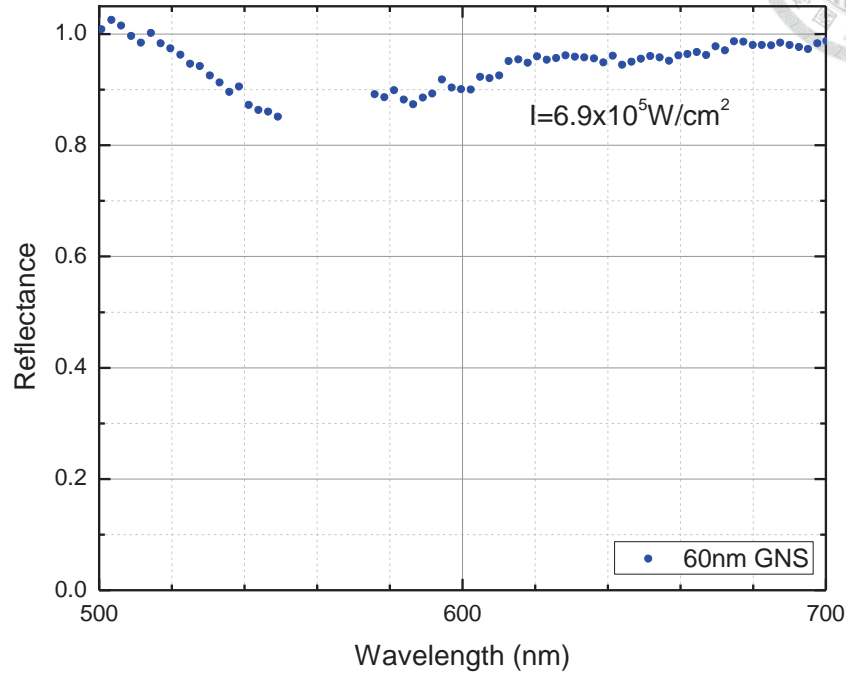


Fig. 4-5 Suppression spectrum of 60nm GNS by CW 561nm laser.

From the spectrum, 60nm GNSs is suppressed less than 80nm GNSs, which is consistent with our size dependency of saturable scattering in section 3.2. We may also plot $1 - \text{Reflectance}$ fitted with the field enhancement (by (2.14)), as Fig. 4-6. Although the peak lies within the band width of notch filter, apparent blue shift of the spectrum compared with 80nm GNSs can still be seen.

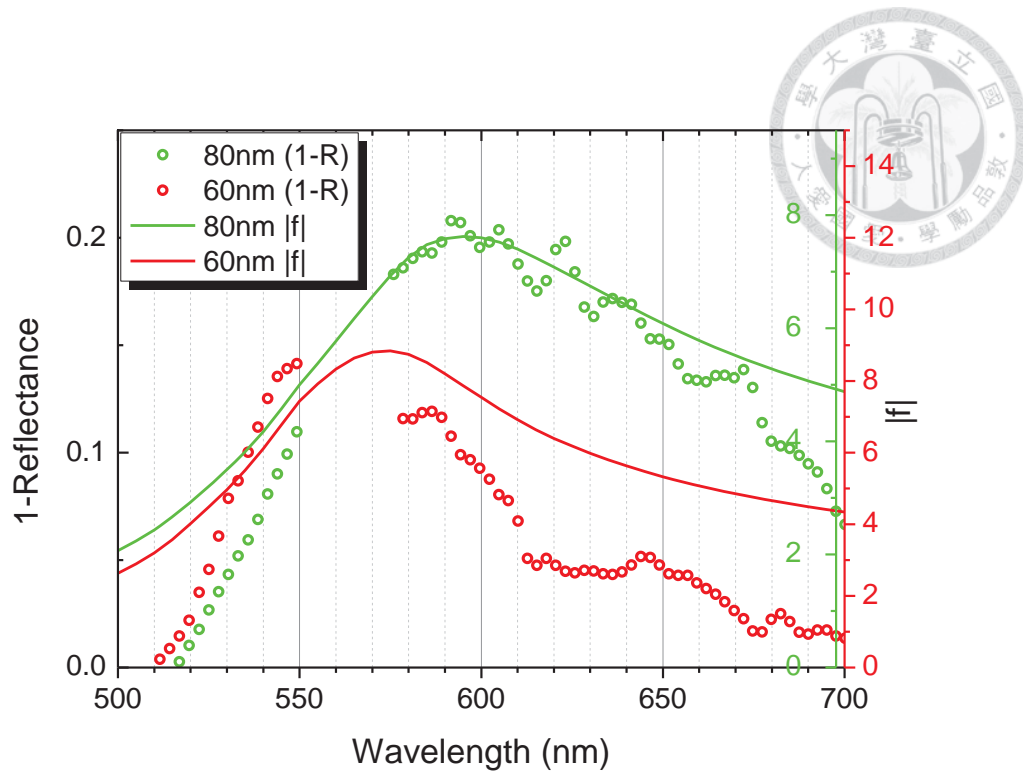
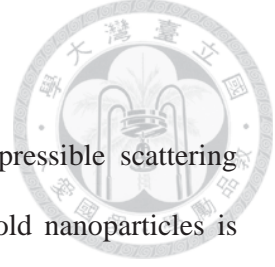


Fig. 4-6 Suppression spectrum (1-Reflectance) fitted with the field enhancement of 80nm and 60nm GNSs

Chapter 5 Microscopic Mechanisms



The wavelength dependencies of saturable (section 3.1) and suppressible scattering (section 4.1) have shown that the nonlinear scattering of single gold nanoparticles is strongly related to localized surface plasmon resonance, which could be understood by $\chi^{(3)}$ model (Chapter 2). However, the microscopic mechanism of $\chi^{(3)}$ is still unknown. In section 1.3, several different possible mechanisms were discussed. In this chapter, we will try to shed some light on it by existent experimental results and literatures.

5.1 Third Order Nonlinear Polarizations

Nowadays, the paradigm to calculate optical constant is through density matrix technique[23] with given states of electrons[24]. For gold, the relevant states in optical region include the s-p band (conduction band) and d-band (valence band). The third order nonlinear polarization, including the third order intraband (within s-p band) and interband transition (between s-p band and d-band), contributes to Kerr $\chi^{(3)}$, as calculated in several papers[18,19]. These kinds of nonlinearities have the lifetime almost the same as excitation of plasmon polariton (few fs), which can be viewed as instantaneous for most of the experiments.

However, if the nonlinear scattering by CW laser is caused by the instantaneous nonlinear polarizations, the same phenomenon should be observed at the comparable peak intensity for pulse laser. To confirm the possibility, we converted 1040nm, 500fs, 43 MHz Yb fiber laser (Uranus 005-500-INS-PM, PolarOnyx Inc., United States) to 520nm pulse laser by second harmonic generation (LBO, Castech, China), and measured the curve of reflectance versus peak intensity. According to the Fig. 3-1, the nonlinearity should occur at $10^6 \sim 10^7 W/cm^2$. Our experimental results, however,

shows that the scattering is linear over the region (Fig. 5-1).

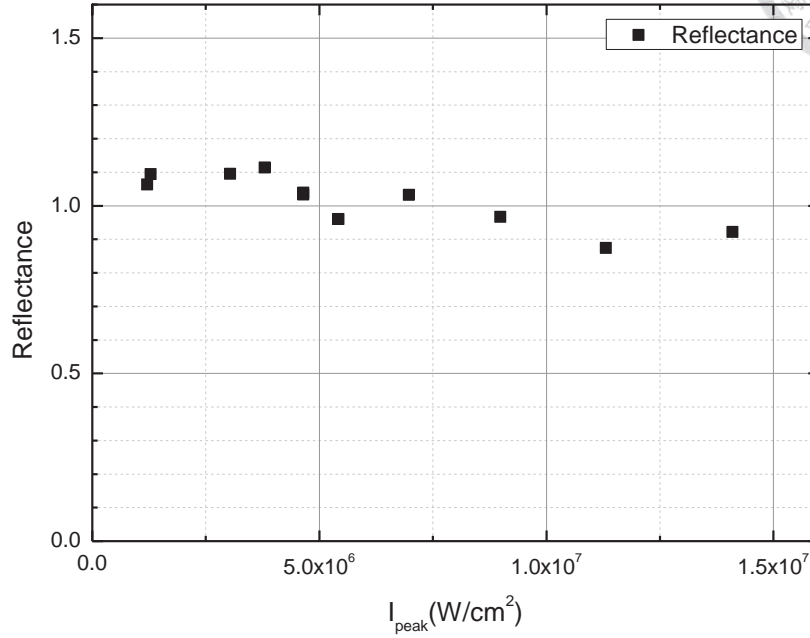


Fig. 5-1 Reflectance v.s. peak intensity for 80nm GNS by 520nm, 500fs pulse laser.

On the other hand, the degenerate four-wave mixing experiments in the literature show that $|\chi^{(3)}| \approx 10^{-17} \sim 10^{-19}$ (SI unit) [18,25,38], which purely comes from instantaneous nonlinear polarization. This value is much smaller than us ($|\chi^{(3)}| \approx 10^{-14} \sim 10^{-15}$ (SI unit) from section 3.1. These reasons show that the instantaneous nonlinear polarizations cannot be the cause of saturable scattering observed here.

5.2 Hot Electron

After the excitation of surface plasmon polariton, the electron-electron coupling will gradually destroy the collective electron motion and the energy distribution will be thermalized to a uniform temperature, in the time scale of 0.5 ps[15]. This is one of the primary contribution for pulse laser experiment, because the electrons will absorb all

energy of single pulse in a very short time, typically 10 fs to few ps[18]. In our experiments, we used continuous wave laser. In order to estimate the thermal effect of electron on dielectric constant, we may estimate the electron temperature by considering the heat reservoirs of electron and lattice, with heat transfer between them.

In the extreme case, assume $\tau_{e-ph} \gg \tau_{e-e}$, so that electrons reach thermal equilibrium instantly compared with the time scale is heat transfer to lattice. Although the assumption is not quite true for gold, this will give us a upper bound of electron temperature, and thus its effect on dielectric constant. Under this assumption, the absorption of photon will be transferred to electron temperature instantly, but relaxed to lattice in the time scale of 1 ps. In thermal equilibrium, we may get the equation of heat transfer rate:

$$\frac{dQ_{e-lattice}}{dt} = \sigma_{abs} \times I \sim \frac{\Delta Q}{\tau_{e-ph}} \sim \frac{Nk\Delta T_{e-lattice}}{\tau_{e-ph}} \quad (4.1)$$

where the σ_{abs} is absorption cross section, I is intensity, ΔQ is the heat needed to be relaxed to reach equilibrium (assuming no light incident), N is the number of hot electron, k is Boltzmann constant, and $\Delta T_{e-lattice}$ is the temperature difference between electron and lattice. We may plug our experimental parameters in (assuming one free charge per atom), and result gives us $\Delta T_{e-lattice} < 2K$. To calculate the change of dielectric constant under the electron temperature, we refer to Hache's paper[18] ($|\frac{\partial \epsilon}{\partial T}| \sim 3 \times 10^{-3} K^{-1}$), which gives us $|\frac{\delta \epsilon}{\epsilon}| < 1\%$. This number is too small for causing the strong optical nonlinearity of saturable and suppressible scattering, where the change of reflectance is of the scale of more about 10%.

We can also compare the absorbed within the electron-phonon relaxation time. By our

typical intensity $\sim 10^6 \text{ W/cm}^2$, $\frac{\text{fluence}}{\text{area}} \sim 10^6 \text{ W/cm}^2 \times 1 \text{ ps} \sim 10^{-6} \text{ J/cm}^2$. In the

literature of saturable absorption, which is largely attributed to hot electron,

$\frac{\text{fluence}}{\text{area}} \approx 10^{-1} \sim 10^{-2} \text{ J/cm}^2$ [20,32]. This shows that our electron temperature should

be smaller than theirs for at least 3 orders of magnitude. Thus, hot electron cannot be the main contribution of them.

5.3 Hot Lattice

After the heat is transferred from electron to lattice, the temperature change of lattice could change the dielectric constant. In the case, the heat comes from the electron-phonon coupling, and is relaxed to matrix. In equilibrium, the temperature rise of the lattice changes the dielectric constant, which gives us the nonlinearity:

$$\begin{aligned} \chi^{(1)}(T) &\approx \chi_r^{(1)}(T_0) + \frac{\partial \chi_r^{(1)}}{\partial T}(T_0) \times \Delta T \\ &= \chi_r^{(1)} + (\text{const.}) \times \sigma_{abs} |E|^2 \\ &= \chi_r^{(1)} + \chi_r^{(3)} |E|^2 \end{aligned} \quad (4.2)$$

In this case, $|\chi_r^{(3)}| \propto \sigma_{abs}$ gives us wavelength dependency of effective $|\chi_r^{(3)}|$. With this dispersive $|\chi_r^{(3)}|$, we may fit the wavelength dependency of saturable scattering as

Fig. 3-1, but replace saturation slope with

$$\begin{aligned} S_{sat} &= -\text{Re} \left[\frac{4f_2^2 |f_2|^2}{3c\epsilon_0 n_M f_1} \chi_r^{(3)} \right] \\ &\sim |f|^3 |\chi_r^{(3)}| \\ &\propto |f|^3 \sigma_{abs} \end{aligned} \quad (4.3)$$

The result is shown in Fig. 5-2, which shows LSPR peak as before. It is hard to tell whether it is better than constant $|\chi_r^{(3)}|$ model from the fitting.

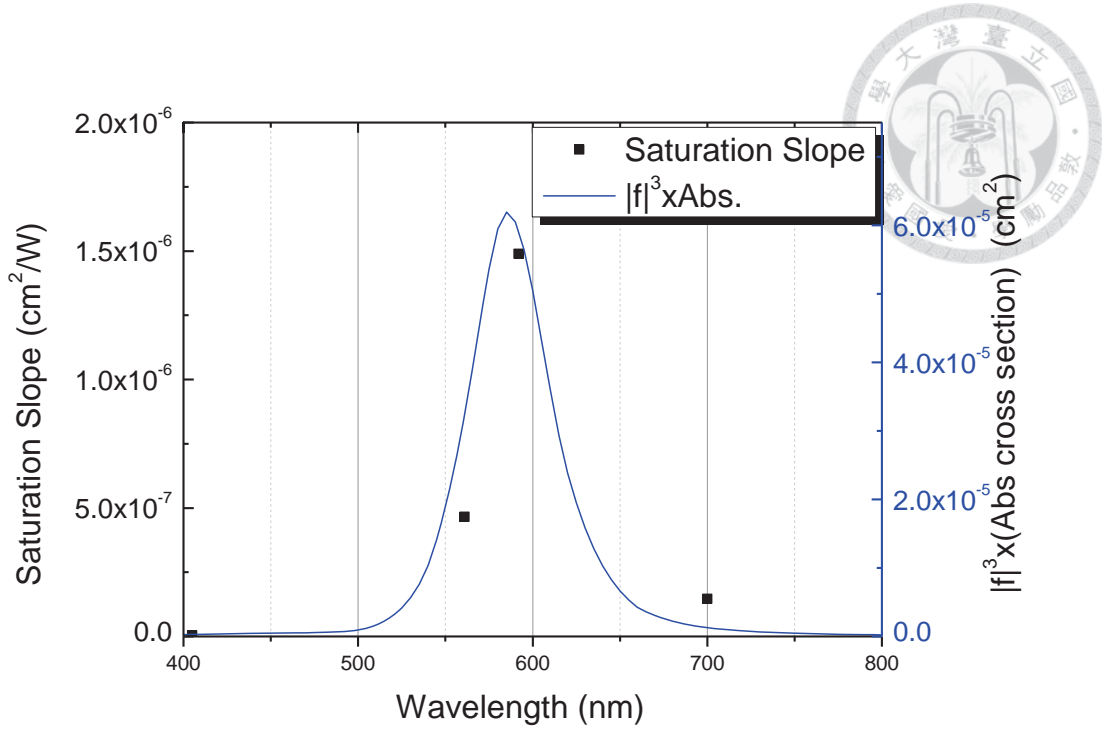


Fig. 5-2 Wavelength dependency of saturable scattering of 80nm GNSs fitted with $\chi_r^{(3)}$ model from hot lattice.

On the other hand, we may make an order-of-magnitude estimation for the temperature changes. According to the same logic as the estimation of electrons' temperature, we may write:

$$\frac{dQ_{\text{lattice-matrix}}}{dt} = \sigma_{\text{abs}} \times I \sim \frac{\Delta Q}{\tau_{\text{ph-m}}} \sim \frac{C \Delta T_{\text{lattice-matrix}}}{\tau_{\text{ph-m}}} \quad (4.4)$$

where the σ_{abs} is absorption cross section, I is intensity, ΔQ is the heat needed to be relaxed to reach equilibrium (assuming no light incident), C is the heat capacitance of gold's lattice, $\Delta T_{\text{lattice-matrix}}$ is the temperature difference between lattice and matrix, and $\tau_{\text{ph-m}}$ is the relaxation time from lattice to matrix. We may plug our experimental parameters in (with intensity = 10^6 W/cm^2 , $\tau_{\text{ph-m}} \sim 100 \text{ ps}$ [14]), and result gives us



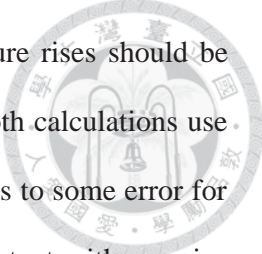
$\Delta T_{lattice-matrix} \sim 100K$. This is consistent with the calculation in the literature using heat transfer equation, which gives the temperature rise of about 400K for 80nm GNS in water under laser intensity of $10^6 W / cm^2$ [35,39].

This is large enough to alter dielectric constant[40]. There is also circumstantial evidence from the temperature dependency of extinction spectrum of GNSs solution, which shows that the absorption will decrease with temperature[34]. Because the absorption and scattering share the same field enhancement factor (equation (1.10)), the decrease of scattering spectrum is also expected. This is also consistent with our suppressed scattering spectrum in Chapter 4. According to all of the reasons above, the temperature rise of GNS itself is the most probable mechanism for the nonlinear scattering observed by CW laser around LSPR peak.

The temperature rise can also explain the size dependency of nonlinearity. According to literature[35,39], larger GNS will reach higher temperature in equilibrium. It is also easy to have a qualitative explanation: in equilibrium, the absorbed energy should be the same as the heat relaxed to matrix. The absorption cross section increases with the volume of GNS (equation (1.10)), which increases the creation of heat. This is compensated by the heat capacitance of GNS, which is also proportional to the volume; On the other hand, considering a two temperature approximation of GNS and matrix, the heat relaxed to matrix should be proportional to the surface area of GNS and the temperature difference between them. In short,

$$a^3 \propto \frac{dQ_{abs}}{dt} = ka^2 \Delta T_{lattice-matrix} \quad (4.5)$$

In result, temperature difference is proportional to radius. In experiment, we didn't directly get this linear behavior. One of the reason is that the two-temperature approximation is too naïve: the temperature of matrix is inversely related to radius in



exact solution calculation[35,39], which gives us that the temperature rises should be proportional to the square of the size of GNS. On the other hand, both calculations use small particle approximation for absorption cross section, which leads to some error for the field enhancement factor. Still, the qualitative behavior is consistent with our size dependency.

In order to confirm the temperature effect on the scattering of GNS, we heated up the GNSs sample by homemade heater with commercial controller (UT150, Yokogawa Electric Corporation, Japan) from 30 to 80 °C, and measure the change of the scattering spectrum of single GNS. Calculating the reflectance normalized by the scattering spectrum at 30°C, we got the results as Fig. 5-3. This result looks very similar to the suppression spectrum (Fig. 4-3), where the decrease of reflectance is largest around LSPR peak. This confirms that the rise of temperature of tens of Celsius degree can be the cause of the nonlinear scattering of single GNS. All of the evidences above make us believe that the hot lattice should be the microscopic mechanism of saturable and suppressible scattering of single gold nanoparticle.

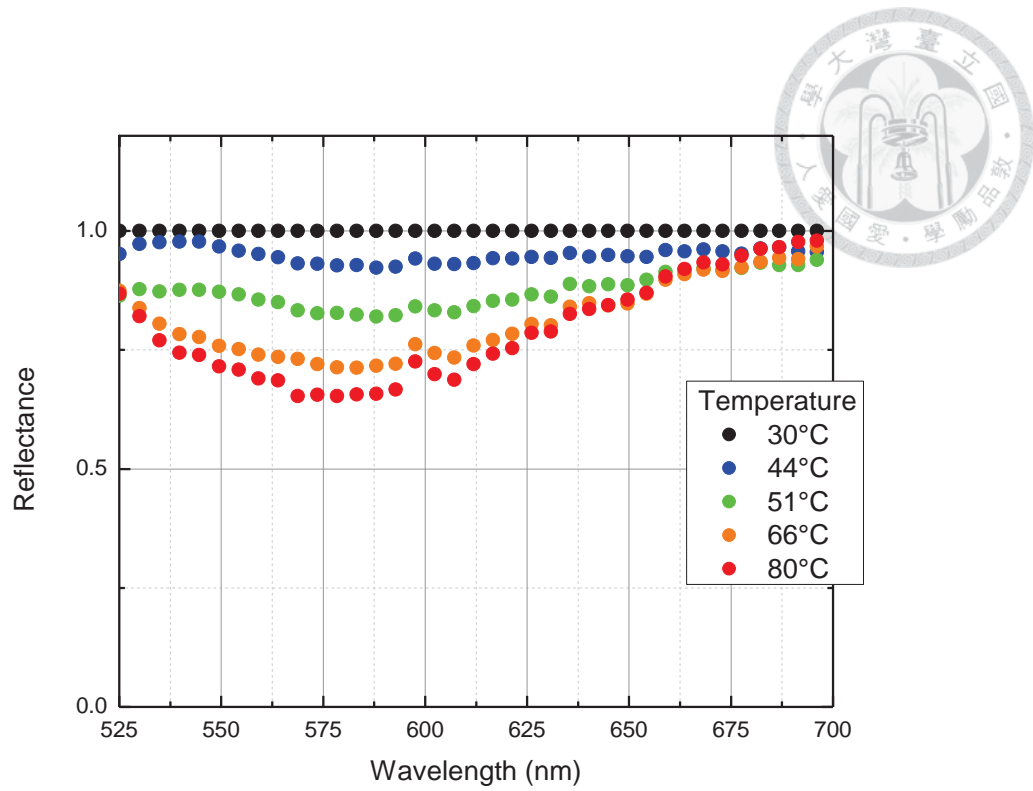
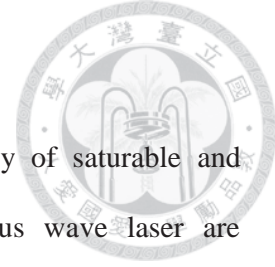


Fig. 5-3 Reflectance of single gold nanosphere at different temperatures, normalized by the scattering spectrum at 30°C.

Chapter 6 Conclusion



In this thesis, the wavelength, size, and polarization dependency of saturable and suppressible scattering of single gold nanosphere by continuous wave laser are measured. The results shows that the optical nonlinearities are strongly related to localized surface plasmon resonance, and the wavelength dependency fits well with $\chi_r^{(3)}$ model. On the other hand, the nonlinearity increases with the size of gold nanosphere, but is independent of polarization of laser beam.

From the pump-probe's experimental results in the literature, we may list the possible sources of nonlinearity. Using sub-ps laser to test the linearity of scattering, we can exclude the possibility of instantaneous nonlinear polarization, including interband and intraband. The contribution from hot electron is also too small to cause the strong nonlinearity by simple order-of-magnitude estimation. The estimated temperature rise of GNS's lattice seems to be a possible reason, which is consistent with the calculation by heat transfer equation in the literature. The scattering spectrum's change with temperature from experiment also supports this mechanism. In conclusion, our results strongly imply that the saturable and suppressible scattering of single GNS observed by continuous wave laser are cause by the temperature rises of lattice, and the nonlinearity is enhanced by localized surface plasmon resonance.

REFERENCE



- [1] S.-W. Chu *et al.*, ACS Photonics, 131115090709009 (2013).
- [2] S.-W. Chu *et al.*, Physical Review Letter **112**, 017402 (2014).
- [3] S.-W. Chu *et al.*, ACS Photonics **1**, 32 (2013).
- [4] M.-C. Daniel and D. Astruc, Chemical Reviews **104**, 293 (2003).
- [5] S. Eustis and M. A. El-Sayed, Chem Soc Rev **35**, 209 (2006).
- [6] C. F. Bohren and D. R. Huffman, *Absorption and scattering of light by small particles* (Wiley, New York, 1983).
- [7] J. D. Jackson, *Classical Electrodynamics* (John Wiley & Sons. Inc., 1998).
- [8] S. Nie and S. R. Emory, Science **21**, 1102 (1997).
- [9] P. B. Johnson and R. W. Christy, Phys Rev B **6**, 4370 (1972).
- [10] B. Hammer and J. K. Norskov, Nature **376**, 238 (2002).
- [11] M. Auffan, J. Rose, M. R. Wiesner, and J. Y. Bottero, Environmental pollution **157**, 1127 (2009).
- [12] C. Voisin, N. Del Fatti, D. Christofilos, and F. Vallee, J Phys Chem B **105**, 2264 (2001).
- [13] J. Y. Bigot, V. Halte, J. C. Merle, and A. Daunois, Chem Phys **251**, 181 (2000).
- [14] S. Link and M. A. El-Sayed, J. Phys. Chem. B **103**, 8410 (1999).
- [15] C. K. Sun, F. Vallée, L. Acioli, E. Ippen, and J. Fujimoto, Phys Rev B **50**, 15337 (1994).
- [16] N. Del Fatti, F. Vallee, C. Flytzanis, Y. Hamanaka, and A. Nakamura, Chem Phys **251**, 215 (2000).
- [17] C. Voisin, N. D. Fatti, D. Christofilos, and F. Vallée, Appl Surf Sci **164**, 131 (2000).
- [18] F. Hache, D. Ricard, C. Flytzanis, and U. Kreibig, Applied Physics A **47**, 347 (1988).
- [19] S. G. Rautian, Journal of Experimental and Theoretical Physics **85**, 451 (1997).
- [20] D. D. Smith, G. Fischer, R. W. Boyd, and D. A. Gregory, J Opt Soc Am B **14**, 1625 (1997).
- [21] L. Francuiois, M. Mostafavi, J. Belloni, J.-F. Delouis, J. Delaire, and P. Fenevrou, (2000).
- [22] S. L. Logunov, T. S. Ahmadi, and M. A. El-Sayed, J Phys Chem B **101**, 3713 (1997).
- [23] Y. R. Shen, *The Principles of Nonlinear Optics* (John Wiley & Sons, Inc, 2003).
- [24] N. Christensen and B. Seraphin, Phys Rev B **4**, 3321 (1971).
- [25] M. J. Bloemer, J. W. Haus, and P. R. Ashley, J Opt Soc Am B **7**, 790 (1990).
- [26] K. Puech, W. Blau, A. Grund, C. Bubeck, and G. Cardenas, Opt Lett **20**, 1613 (1995).
- [27] D. Ricard, P. Roussignol, and C. Flytzanis, Opt Lett **10**, 511 (1985).
- [28] E. J. Heilweil and R. M. Hochstrasser, The Journal of Chemical Physics **82**, 4762 (1985).
- [29] K. Puech, F. Z. Henari, W. J. Blau, D. Duff, and G. Schmid, Chem Phys Lett **247**, 13 (1995).
- [30] C. K. Sun, F. Vallée, L. Acioli, E. Ippen, and J. Fujimoto, Phys Rev B **48**, 12365 (1993).
- [31] H. I. Elim, J. Yang, J. Y. Lee, J. Mi, and W. Ji, Appl Phys Lett **88**, 083107 (2006).
- [32] S. L. Qu *et al.*, Chem Phys Lett **368**, 352 (2003).
- [33] W. Fann, R. Storz, H. Tom, and J. Bokor, Phys Rev B **46**, 13592 (1992).

- [34] S. Link and M. A. El-Sayed, *J. Phys. Chem. B* **103**, 4212 (1999).
- [35] A. O. Govorov, W. Zhang, T. Skeini, H. Richardson, J. Lee, and N. A. Kotov, *Nanoscale Research Letters* **1**, 84 (2006).
- [36] K. Fujita, M. Kobayashi, S. Kawano, M. Yamanaka, and S. Kawata, *Physical review letters* **99**, 228105 (2007).
- [37] R. W. Hellwarth, *Progress in Quantum Electronics* **5**, 1 (1977).
- [38] H. Inouye, K. Tanaka, I. Tanahashi, and K. Hirao, *Jpn J Appl Phys* **37**, 1520 (1998).
- [39] H. Goldenberg and C. J. Tranter, *British Journal of Applied Physics* **3**, 296 (1952).
- [40] G. P. Pells and M. Shiga, *J. Phys. C: Solid State Phys.* **2**, 1835 (1969).

